Research Paper

Host immunosenescence compromises *Mycobacterium tuberculosis* clearance

Falak Pahwa[1], Shweta Chaudhary[1], Ashish Gupta[1], Shivam Chaturvedi[2], Ranjan Kumar Nanda[1]

[1]Translational Health Group, International Centre for Genetic Engineering and Biotechnology, New Delhi, 110067, India
[2]Bio-experimentation Facility, International Centre for Genetic Engineering and Biotechnology, New Delhi, 110067, India

Correspondence to: Ranjan Kumar Nanda; **email:** ranjan@icgeb.res.in
Keywords: aging, tuberculosis, immunosenescence, T_{FH} cells, proteomics
Received: September 30, 2025 **Accepted:** April 16, 2026 **Published:** May 4, 2026

ABSTRACT

Immunosenescence increases susceptibility to infectious diseases like tuberculosis (TB) in older adults (≥60 years) and hinder effective containment of *Mycobacterium tuberculosis* (Mtb) during therapeutic intervention. A comprehensive understanding of the cellular and molecular changes underlying age-associated immune alterations may inform development of strategies to improve treatment outcomes. Here, we monitored the immunopathology, frequency, and functionality of immune cells across extreme age groups of C57BL/6 mice following low aerosol dose infection (100-120 cfu) with Mtb H37Rv and treatment with rifampicin and isoniazid (RIF-INH). Up to 6 weeks post infection, mycobacterial load in tissues (lung, spleen, and liver) of old (17-19 months; M) and aged (31M) C57BL/6 mice was similar to that of young (2-4M) mice. However, at two weeks post-treatment, older mice showed a slower rate of Mtb clearance in the lungs. Mtb-infected old mice had higher splenic T-follicular cytotoxic (T_{FC})-like cells, and proteomic analysis of flow-sorted $CD4^+CD44^+$ T cells revealed deregulated mitochondrial proteins (4-hydroxy-2-oxoglutarate aldolase, aspartate aminotransferase, and prostaglandin E synthase), suggesting impaired mitochondrial function. Collectively, these findings suggest that age-associated immune alterations may disrupt immunometabolic pathways, thereby contributing to the delayed Mtb clearance. Targeting immunometabolic dysfunction therefore represents a promising strategy to enhance TB treatment efficacy and reduce disease burden in older populations.

INTRODUCTION

A recent WHO report predicts that, by 2030, one in six people globally will be over 60 years of age [1]. Aging profoundly impairs immune competence, a phenomenon termed immunosenescence, rendering older adults (≥60 years) highly vulnerable to infectious diseases such as tuberculosis (TB) [2]. *Mycobacterium tuberculosis* (Mtb), the causative pathogen of TB, induces hypermethylation and transcriptional reprogramming of host immune cells, further exacerbating age-related immune dysfunction [3]. Clinically, older adults exhibit reduced vaccine effectiveness alongside heightened susceptibility to TB, with epidemiological data indicating 2-3 times higher TB incidence and up to four times higher mortality than younger patients. In several East Asian regions, including Japan, Korea, and Hong Kong, older adults accounted for 45-69% of TB cases in 2020-21 [4]. Similarly, projections from Taiwan predict 78% of new TB cases by 2035 will arise in the geriatric population, which currently contributes to 82.1% of TB-associated mortality [5, 6]. These trends underscore the urgent need to elucidate age-associated immune defects driving TB vulnerability in an aging world.

Despite this growing burden, current TB research predominantly employs young adult mouse models (6-8 weeks old, equivalent to ~18-year-old humans), which do not adequately capture the immune landscape of older hosts [7]. Evidence from studies suggests that old (>18 months; M) mice exhibit higher bacterial burden, delayed $CD4^+$ T cell responses, and altered immune activation compared to younger counterparts [8, 9, 10]. However, the impact of immunosenescence on bacterial clearance dynamics, immune cell phenotypes, and host responses during TB treatment remain largely unexplored.

To address this knowledge gap, we investigated age-dependent effects on Mtb infection and treatment in C57BL/6 mice spanning young (2-4M), mid-aged (9-12M; 38-44 human years), old (17-19M; ~54-60 human years), and aged (31M; >80 human years) stages. Following low-dose aerosol infection with Mtb H37Rv and treatment with rifampicin and isoniazid (RIF-INH), we monitored bacterial clearance kinetics across tissues, profiled systemic and tissue-specific immune responses, including circulating cytokines, Mtb-specific antibodies, liver micronutrients, and the proteome of splenic $CD4^+CD44^+$ T cells. Through this approach, we aimed to identify age-associated processes that compromise treatment efficacy, which can inform strategies to reduce the risk of relapse in geriatric TB patients.

RESULTS

Lung Mtb burden in C57BL/6 mice remains unaffected by age or sex through 6 weeks post-infection

The influence of host age and sex on susceptibility to Mtb infection remains an area of interest, particularly at early time points. Thus, female and male C57BL/6 mice of wider age groups were aerosol infected with a low dose of H37Rv (Figure 1A). Mice were categorized as young (2-4M), middle-aged (9M females, 12M males) and old (17-19M males). Prior to Mtb infection, body weight was higher in middle-aged and older mice than in younger controls (Supplementary Figure 1). During the study period, old mice lost ~3% weight, whereas young mice gained ~8% weight (Figure 1B). Young female mice gained more body weight (~20%) than males (~10%) (Figure 1B). At 6 weeks post infection (w.p.i.), middle-aged male mice showed significant body weight loss (Figure 1B). Despite age-related variations in body weight, lung Mtb burden progressively increased up to 4 w.p.i. before plateauing by 6 w.p.i., with no significant differences attributable to age or sex (Figure 1C). Thus, immunosenescence manifests primarily during therapeutic clearance rather than initial containment phase, rationalizing our focus on age-associated differences in treatment response.

Inflammaging and immune defects drive delayed TB clearance in aging despite hepatic resilience

To evaluate the impact of age on treatment response, a subset of mice received RIF-INH following Mtb infection. Remarkably, older mice retained a significantly higher ~3 $\log_{10}$ cfu lung Mtb load at 2 weeks post-treatment (w.p.t.) compared to the young group (~1.5 $\log_{10}$ cfu). And by 4 weeks, both mouse age groups achieved complete bacterial clearance, i.e. resulting below the limit of detection (LOD) (Figure 2A, 2B). Histologically, old mice developed granulomatous lung lesions with prominent foamy cells later (6 w.p.i.) compared to young mice (4 w.p.i.) (Supplementary Figure 1). Lung inflammation was resolved in young mice by 4 w.p.t. but persisted in old mice (Supplementary Figure 1). Additionally, middle-aged mice were able to resolve the inflammation by 4 w.p.t., irrespective of sex (Supplementary Figure 2). In extrapulmonary sites, such as spleen and liver, mycobacterial clearance was observed by 2 w.p.t. in both age groups (Figure 2B).

Liver enzymes are pivotal for drug metabolism, with metal ions exerting substantial influence over their activity. Age-related changes may influence this variability in liver function and micronutrient status [11]. Thus, we monitored the liver micronutrient levels of these mouse groups using inductively coupled plasma mass spectrometry (ICP-MS) (Supplementary Figure 3). Old mice had higher hepatic Cu (4.28×), low Zn (0.14×) levels with similar Fe and Se levels compared to controls (Supplementary Figure 3). Additionally, old mice receiving treatment showed higher hepatic Cu levels (Supplementary Figure 3). Liver micronutrient status impacts activities of hepatic enzymes like alanine aminotransferase (ALT) and aspartate aminotransferase (AST), commonly used markers of liver function and injury. Old mice exhibited comparable serum ALT and AST activities to the young mice (Figure 2C). However, ALT activity showed a non-significant upward ($p=0.06$) trend in old mice (Figure 2C). Mtb infection did not impact serum AST or ALT activity in old mice, but ALT activity was higher in Mtb-infected younger mice (Figure 2C). Strikingly, young mice receiving treatment had higher serum AST activity reflecting drug-induced liver injury, while old mice remained unaffected (Figure 2C).

To assess age-related differences in humoral immunity against Mtb, if any, serum anti-H37Rv specific IgG titers were measured. The overall IgG response was

significantly higher in old mice compared to young mice (Figure 2D). Importantly, old mice receiving treatment mounted higher IgG responses at a later time point i.e. 4 w.p.t., while young mice showed it at 2 w.p.t. compared to their respective infected controls (Figure 2D and Supplementary Figure 4). While robust humoral responses are beneficial for pathogen control, the delayed yet heightened antibody response in old mice could indicate persistent antigenic stimulation and likely reflect altered immune regulation with aging. Circulatory IL-6 levels were higher in old mice, consistent with a state of chronic low-grade inflammation or inflammaging (Figure 2E). Higher circulatory IFN-γ levels were observed in Mtb-infected young and old mice, which resolved partially in treated groups (Figure 2E). The cytokine response in old mice appears skewed toward a T_H1-type response rather than a broad systemic inflammatory state, which may explain selective upregulation of IFN-γ without a parallel increase in IL-6. However, at the site of infection, IFN-γ levels trended higher in young mice compared to old mice (Figure 2F). Critically, despite RIF-INH treatment selectively reducing lung IFN-γ levels in old mice, yet bacterial clearance remained impaired (Figure 2F). This reveals a central paradox showing T_H1 contraction coupled with effector dysfunction, where diminished IFN-γ, rather than unresolved inflammation, impairs bacterial killing during early therapy.

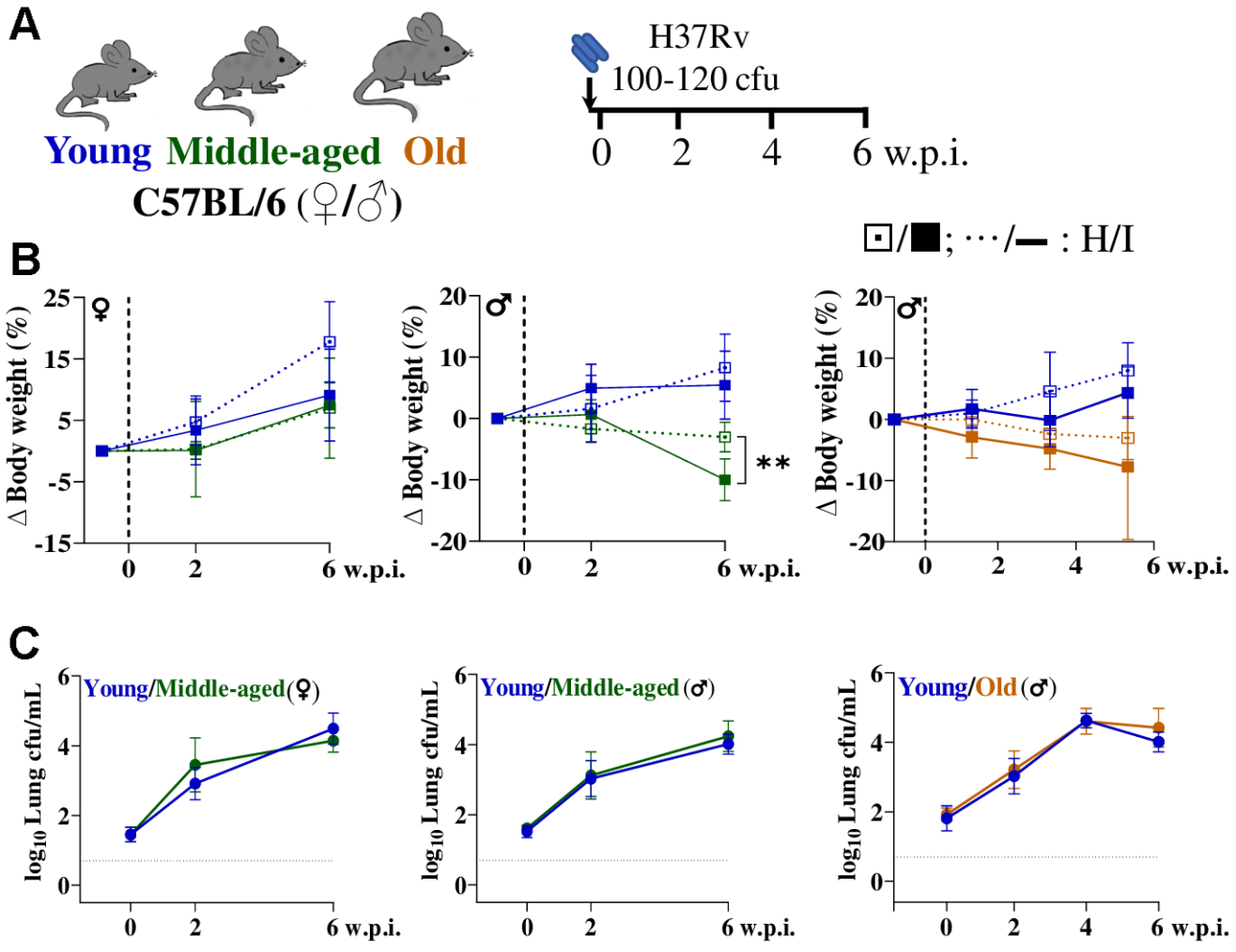

Figure 1. Lung Mtb burden remains similar till 6 weeks post-infection across age groups and sexes in C57BL/6 mice. (**A**) Schematic of the experimental design used for aerosol Mtb H37Rv infection of C57BL/6 mice [female (♀) and male (♂)] across age groups. (**B**) Changes in body weight of mice groups (healthy: H, ⋯; infected: I, —) are presented, n=5-10/age group/condition; dashed vertical line represents day of infection. (**C**) Lung bacterial burden (in log_{10}cfu/mL) in mice post Mtb infection; n=5-10/timepoint/age group/condition; dashed horizontal line represents limit of detection (LOD). Young (2-4 months) in blue, middle-aged (9-12 months) in green and old (17-19 months) mice in brown; cfu= colony forming unit; w.p.i.= weeks post infection; p-value: ** <0.005 at 95% confidence interval by Mann-Whitney test. Data shown as mean ± SD. See also Supplementary Figures 1, 2.

Age-related T cell dysregulation impairs immune Mtb control

$CD4^+$ T cells control Mtb primarily by producing cytokines and licensing infected phagocytes, but aging drives progressive dysfunction marked by exhaustion-like phenotypes. T cells were profiled using activation markers (CD44, PD1), homing receptor (CXCR5), senescence (KLRG1, CD153) and lineage-defining transcription factors (Tbet for T_H1 and FoxP3 for T_{reg}) and a significant change in their distribution was observed in old mice (Supplementary Figure 5). CD44hi marks antigen-experienced $CD4^+$ T cells, while PD-1 captures chronically stimulated cells that can be either functional (protective, $CXCR5^+$ T_{FH}-like) or dysfunctional depending on expression of other

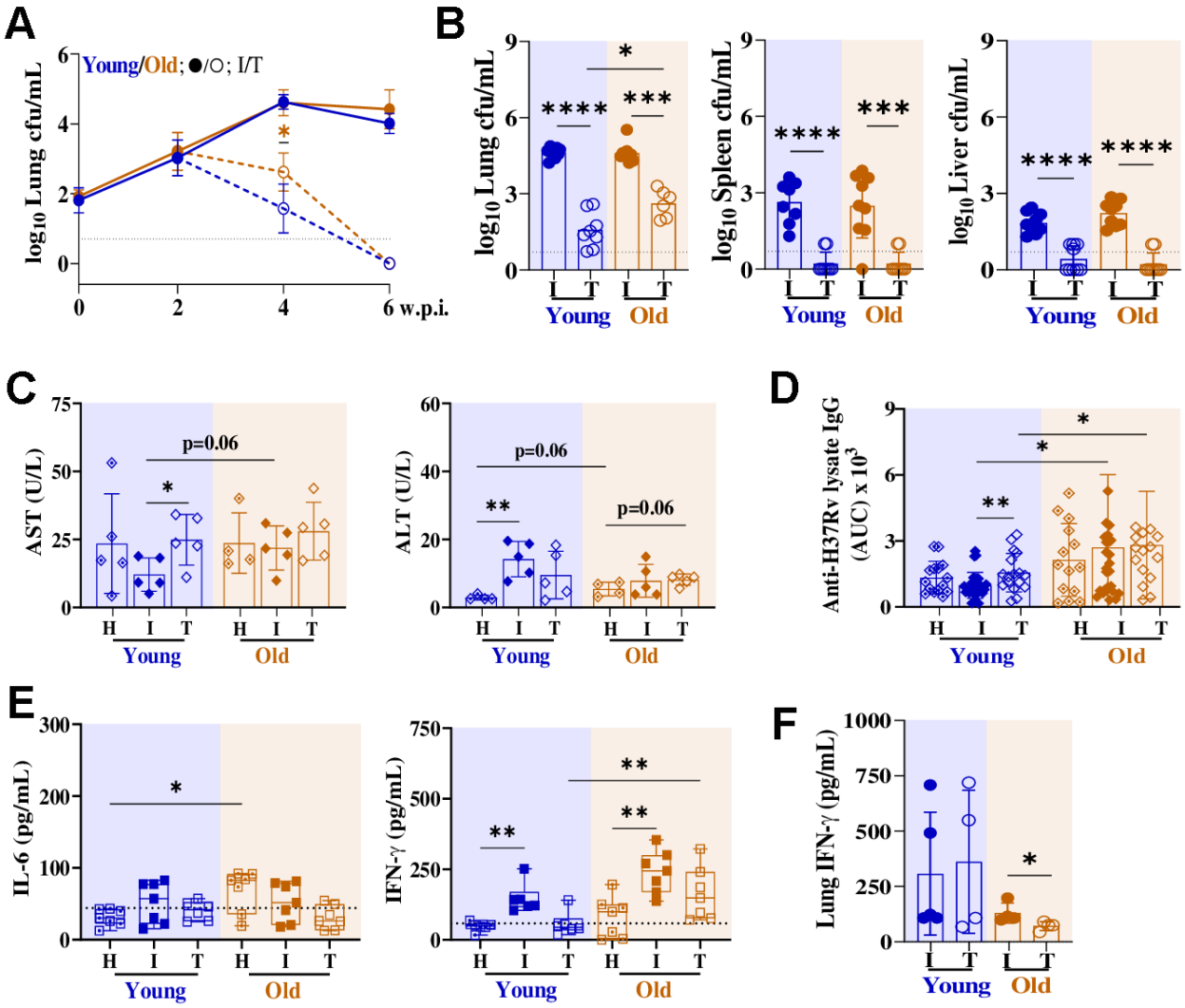

Figure 2. Old C57BL/6 mice exhibit delayed lung Mtb clearance following two weeks of RIF-INH treatment. (**A**) Lung bacterial burden (in log_{10}cfu/mL) in male C57BL/6 mice from infected (I; at 2, 4 and 6 w.p.i.) and treated (T; at 2 and 4 w.p.t.; treatment started at 2 w.p.i.) groups; n=10/timepoint/age group/condition; dashed horizontal line represents limit of detection (LOD). A set of two independent experiments is depicted. (**B**–**F**) showing data of infected groups at 4 w.p.i. and treated groups at 2 w.p.t.. **(B)** Bacterial load (in log_{10}cfu/mL) in lung, spleen and liver; individual data points at 4 w.p.i./2 w.p.t. presented in histograms (n=10/age group/condition). (**C**) Serum alanine transaminase (ALT) and aspartate aminotransferase (AST) activities in mice of different groups (n=5/age group/condition) at 4 w.p.i./2 w.p.t.. (**D**) Area under the curve (AUC) for Mtb H37Rv lysate-specific serum IgG in healthy (H; n=15/age group), infected (I; n=27-28/age group) and treated (T; n= 16-17/age group) mice at 4 w.p.i./2 w.p.t.. (**E**) Serum cytokines (in picogram per milliliter): IL-6, IFN-γ in different mice groups (n=6-7/age group/condition) at 4 w.p.i./2 w.p.t.. (**F**) Lung IFN-γ in the different mice groups (n=4-5/age group/condition) at 4 w.p.i./2 w.p.t.. Young (2-4 months) in blue and old (17-19 months) mice in brown; cfu= colony forming unit; w.p.i.= weeks post infection; w.p.t.= weeks post treatment; p-values: * ≤0.05, ** <0.005, *** <0.0005 and **** <0.0001 at 95% confidence interval by Mann-Whitney test. Data shown as mean ± SD. See also Supplementary Figures 1, 4.

markers. $CXCR5^+CD4^+$ T cells support B cell help and are associated with better Mtb control when present in organized structures [12, 13]. KLRG1 is enriched on highly differentiated, senescent-like $CD4^+$ T cells that accumulate with age. $KLRG1^+PD1^+$ T represents late-differentiated, senescent-like cells with constrained effector function. Notably, high expression of CD44, CXCR5, PD1 and CD153 in $CD4^+$ and $CD8^+$ T cells of old mice were observed (Supplementary Figure 5, 6). Increased circulatory $CD4^+KLRG1^+PD1^+$ cells were observed in old mice, indicative of a higher frequency of exhausted T cell phenotype (Supplementary Figure 5).

Next, we monitored the immune cell distribution in lungs and spleen of Mtb-infected and RIF-INH treated mice groups (Figure 3A, 3B and Supplementary Figure 7). Old mice showed a lower proportion of splenic $CD4^+$, higher $CD8^+$ T cells, along with higher CXCR5 and PD1 expression compared to young mice (Figure 3C and Supplementary Figure 7). Interestingly, lungs of old mice showed accumulation of $CD4^+CD44^+CXCR5^+$ (T_{FH})-like cells, similar to young mice post Mtb infection (Supplementary Figure 8). Additionally, $CD8^+CD44^+CXCR5^+$ (T_{FC})-like cells were observed to be more abundant in the lungs and spleens of Mtb-infected old mice at 4 w.p.i. (Figure 3C and Supplementary Figures 7, 8). T_{FC}-like cells are a follicular, B-cell interacting CD8 subset, which compete with T_{FH} cells for germinal centre reactions, disrupting antibody maturation.

In a separate experimental set, at 4 w.p.i., lung Mtb load was found to be similar between young (2M) and aged (31M) male C57BL/6 mice groups (Supplementary Figure 9). Old and aged mice had overall higher splenic $CD4^+CD44^+CXCR5^+PD1^+$, $CD4^+CD44^+CXCR5^+PD1^+$ $ICOS^+$ and $CD8^+CD44^+CXCR5^+PD1^+$ cells compared to young mice, irrespective of infection and treatment status (Figure 3C and Supplementary Figure 9). The detailed distribution of immune cells observed in multiple tissues of 2-, 4-, 17-, 19-, and 31M old mice groups is tabulated in Supplementary Table 1. Immuno-senescence creates pathological T_{FH}-T_{FC} competition, diverting adaptive immunity toward dysregulated $CD8^+$ follicular responses that compromise TB therapeutic efficacy.

Splenic T cell proteome reveals age-specific mitochondrial collapse

To further elucidate the molecular drivers of delayed Mtb clearance, we conducted global proteomic profiling of flow-sorted $CD4^+CD44^+$ T cells (Figure 3D and Supplementary Table 2). In set-I, 109 proteins were identified, and Mtb-infected young and old mice showed 23 and 30 deregulated ($p \leq 0.1$, log_2fold change (log_2fc): I/H > |0.58|) proteins, respectively (Figure 3E, 3F and Supplementary Figure 10 and Supplementary Table 3). In set-II, out of 41 identified proteins, ~20 were deregulated in the mouse groups receiving RIF-INH treatment (Figure 3G, 3H and Supplementary Table 4). Proteins involved in immune response (e.g., complement, serotransferrin) were suppressed in old mice, potentially reflecting age-related immune decline. Young mice exhibited few changes, with upregulation of stress response proteins like galectin-1 and superoxide dismutase, possibly reflecting a more robust acute response (Supplementary Table 3). Both mouse age groups showed downregulation of 4-hydroxy-2-oxoglutarate aldolase (HOGA), suggesting disrupted hydroxyproline degradation [14] (Supplementary Table 3). Upon Mtb infection, old mice showed an upregulation of prostaglandin E synthase 3 (PTGES3, log_2fc: I/H = 1.15), indicating an age-biased induction of prostaglandin synthase E2 (PGE2) machinery (Supplementary Table 3). PGE2 disrupts alveolar macrophage metabolic fitness through mitochondrial dysfunction, suppressing electron transport chain gene expression [15].

Additionally, old mice showed elevated levels of mitochondrial AST after treatment (log_2fc: T/I = 3.15), indicative of unresolved mitochondrial stress, consistent with increased serum AST and altered hepatic micronutrient status observed earlier (Supplementary Table 4). Old mice showed lower HOGA abundance after treatment, implying prolonged mitochondrial stress in T cells of old mice (Supplementary Table 4). Together, these proteomic signatures reveal age-specific mitochondrial defects, providing a molecular basis for T cell dysfunction, inflammaging, and impaired myco-bacterial clearance in older hosts, linking cellular metabolic stress in T cells during Mtb infection and therapy.

DISCUSSION

As the global demography is shifting towards the older (≥60 years) age groups, it is expected that immuno-senescence and lack of an effective TB vaccine for adults will be key drivers for the elevated numbers of geriatric TB patients. Paradoxically, in countries where TB was contained successfully, the number of new TB cases is increasing, for example, in Kansas City and North Carolina in the United States. The majority of published reports focused on understanding host-pathogen interactions in Mtb-infected mice of 6-8 weeks (~2M), representing a human age equivalence of 18-20 years [7]. Thus, understanding how the older host responds to Mtb infection is crucial for developing appropriate and effective interventions.

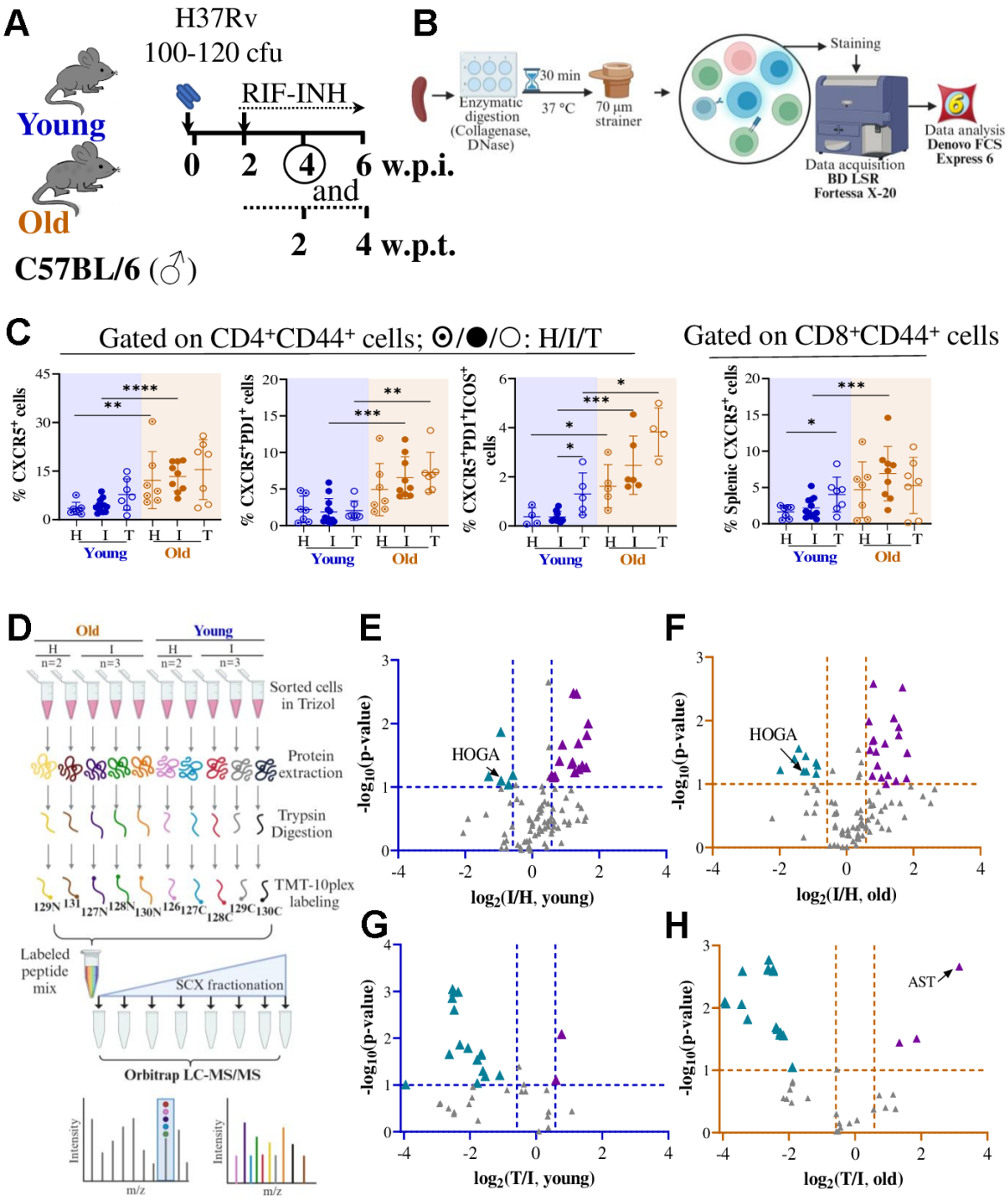

Figure 3. Deregulated splenic CD4⁺CD44⁺ T cell proteome in old C57BL/6 mice upon Mtb infection and RIF-INH treatment. (**A**) Schematic showing Mtb H37Rv aerosol infection in male C57BL/6 mice of two age groups (young: 2-4 and old: 17-19 in months) followed by treatment with RIF-INH starting at 2 w.p.i.. (**B**) Workflow for immune cell isolation from the spleen, flow cytometry data acquisition and data analysis. (**C**) Frequencies of CD4⁺CD44⁺CXCR5⁺, CD4⁺CD44⁺CXCR5⁺PD1⁺ and CD4⁺CD44⁺CXCR5⁺PD1⁺ICOS⁺ and CD8⁺CD44⁺CXCR5⁺ cells in the spleen of C57BL/6 mice at 4 w.p.i./2 w.p.t.. Healthy (H; n=3/age group), infected (I; n=6-10/age group) and treated (T; n=3/age group). (**D**) TMT10plex workflow for CD4⁺CD44⁺ T cell proteome analysis (for TMT set-1) by liquid chromatography- mass spectrometry (LC-MS/MS). (**E**–**H**) showing volcano plots of splenic CD4⁺CD44⁺ T cell proteome showing significantly deregulated proteins (in $-\log_{10}$p-value ≥ 1; $\log_2$fold change > |0.58|): (**E**) Young infected versus healthy, (**F**) Old infected versus healthy, (**G**) Young treated versus infected and (**H**) Old treated versus infected; ▲/▲: up-/down-regulation; HOGA: 4-hydroxy-2-oxoglutarate aldolase; AST: aspartate aminotransferase. Young (2-4 months) mice in blue and old (17-19 months) mice in brown; cfu= colony forming unit; w.p.i.= weeks post infection; p-values: * ≤0.05, ** <0.005, *** <0.0005 and **** <0.0001 at 95% confidence interval by Mann-Whitney test. Data shown as mean ± SD. See also Supplementary Figures 7–10 and Supplementary Tables 1–4.

TB demonstrates a marked gender disparity, with males showing increased susceptibility, with male to female ratio of 1.7 in TB prevalence, which is associated with reduced B cell follicle formation in the lung [16–18]. On the contrary, females exhibit increased T cell activity, production of T_H1-type cytokines, particularly IFN-γ, and robust antibody responses [19]. Above 65 years of age, genomic disparities between the sexes become more pronounced, with males exhibiting higher innate and pro-inflammatory activity [20]. Thus, we focused on using old male mice to study the outcomes upon Mtb infection and post-treatment.

A low aerosol dose of Mtb infection to young (2-4M), middle-aged (9, 12M), old (17-19M) and aged (31M) C57BL/6 mice yielded similar lung mycobacterial burden up to 6 w.p.i.. Whereas earlier reports showed better Mtb control in older mice at earlier time points [8, 9, 21, 22]. Turner et al. reported that 18M C57BL/6 mice aerosol-infected with Erdman strain had a lower lung load at 14 d.p.i., compared to 3M controls [9]. 24M B6D2F1 hybrid mice infected with H37Rv showed lower load at 20 d.p.i. than young 2M controls [8]. Variations in reported tissue Mtb loads between earlier reports and this study may stem from differences in mouse strain and sex, Mtb strain and dose, infection method, and observation timing. Important to highlight that, to the best of our knowledge, this report demonstrates for the first time, that old mice showed a compromised Mtb clearance after 2 weeks of RIF-INH treatment compared to younger controls. These results corroborate the reported delayed viral clearance in 17M BALB/c mice infected with PR8 influenza virus [23].

Aging also impacts hepatic function, affecting the metabolism of exogenous molecules, thereby leading to hepatoxicity [24]. Old mice displayed a higher hepatic Cu/Zn ratio irrespective of infection status, consistent with reports that an elevated Cu/Zn ratio in aged hosts is a biomarker of chronic inflammation and oxidative stress. The accumulation of Cu and Zn in phagosomes increases bactericidal activity; however, Cu overload is detrimental to the host [25]. Low Zn levels in older mice may impair Cu/Zn superoxide-dismutase function, leading to pro-inflammatory effects and weakened hepatic function [26]. Mtb pathogenesis depletes the available Fe pool and is a typical host response in counteracting Mtb replication in TB patients [27]. The liver Fe level was reduced in young mice post-treatment; however, treated old mice retained a higher hepatic Fe pool, providing a niche that could support Mtb growth and persistence. Dysregulated iron homeostasis could influence bacterial burden partly through effects on ferroptosis, which is an important avenue for future mechanistic work. Hepatic micro-nutrient imbalances in old mice did not translate to significant serum ALT/AST elevations or drug-induced liver injury, unlike in young treated mice. This hepatic resilience underscores that age-related treatment delays stem from immune defects rather than metabolic or toxic limitations. Young mice maintained high lung IFN-γ to drive rapid bacterial killing while old mice exhibited premature T_H1 contraction, creating a confluence of impairments during early-phase treatment.

Immune cells, such as $CD4^+$ T cells play a critical role in controlling Mtb, and their function might be partially impaired in older hosts [28]. A higher lung mycobacterial load was predicted in 18M mice at 6 w.p.i. compared to 3M mice, due to a delayed $CD4^+$ T cell response [28, 29]. We observed that Mtb-infected old C57BL/6 mice had similar T_{FH}-like cells in the lungs and a higher frequency in the spleen at 4 w.p.i. compared to younger controls. However, a higher proportion of T_{FC}-like cells was observed in the lungs and spleens in Mtb-infected old mice. The contribution of T_H1 cells in TB is well established. However, our understanding of T_{FH} cells, which link humoral and adaptive immunity, during Mtb infection is limited [30]. T_{FC} cells suppress T_{FH} cell helper function and antibody responses through multiple mechanisms, thereby inhibiting antibody production to maintain self-tolerance and regulate immune responses [31, 32]. Age is reported to negatively influence T_{FH} cell function and differentiation, thereby compromising host responses [33]. Localization of T_{FH}-like cells has been demonstrated within protective granuloma-associated lymphoid tissue in lungs of 2M C57BL/6 mice, which mediates Mtb control [34]. In effective responses, T_{FH} cells dominate the follicular niche, provide IL-21 and CD40L to B cells, and help structure organized germinal centres or tertiary lymphoid-like granulomas. Immuno-senescence drives this pathological skew: aging-associated T_{FH} cells enable T_{FC} expansion, disrupting germinal centre formation and granuloma organization.

Understanding tissue-level T cell distribution in Mtb-infected old mice has been attempted earlier; however, limited reports captured the changes during TB treatment [8, 9, 21, 28, 30]. At 2 w.p.t., young mice showed increased splenic T_{FH}-like cells, which remained similar in old mice, suggesting the inability of the older host to elicit a proper T_{FH} response. Compromised Mtb clearance in old mice might be due to the impaired T_{FH} cell functionality, which was reported earlier in >20M old C57BL/6 mice [12, 33]. Future work should phenotypically characterize T_{FC}-like cells to test their active suppression of protective T_{FH} responses, establishing causality in age-dependent humoral dys-regulation.

Proteome analyses of splenic cells from Mtb-infected old mice revealed altered abundance of mitochondrial enzymes involved in the catabolism of hydroxyproline (Hyp), a product of protein degradation, notably higher AST and lower HOGA [14] (Figure 4). AST catalyzes 4-hydroxy glutamate (4-OH-Glu) to 4-hydroxy-2-oxo-glutarate (HOG), which is converted into pyruvate and glyoxylate using HOGA. This imbalance likely causes HOG accumulation, inhibiting glyoxylate reductase and promoting excessive oxalate production, known to disrupt mitochondrial function independent of the lactate dehydrogenase pathway [35]. PTGES3 upregulation in Mtb-infected old mice further implicates prostaglandin E2 signaling, which prior work shows hampers alveolar macrophage proliferation and mitochondrial function in 18-22M mice [15]. These proteomic changes represent immunometabolic signatures of T cell dysfunction in Mtb-infected old mice rather than as direct causal drivers. The observed HOGA downregulation and PTGES3 signaling likely underlies defective $CD4^+$ T cell responses and impaired Mtb clearance. This aligns with evidence that mitochondrial rescue strategies enhance TB immunity in older adults, positioning mitochondrial axis as a therapeutically actionable target [36, 37].

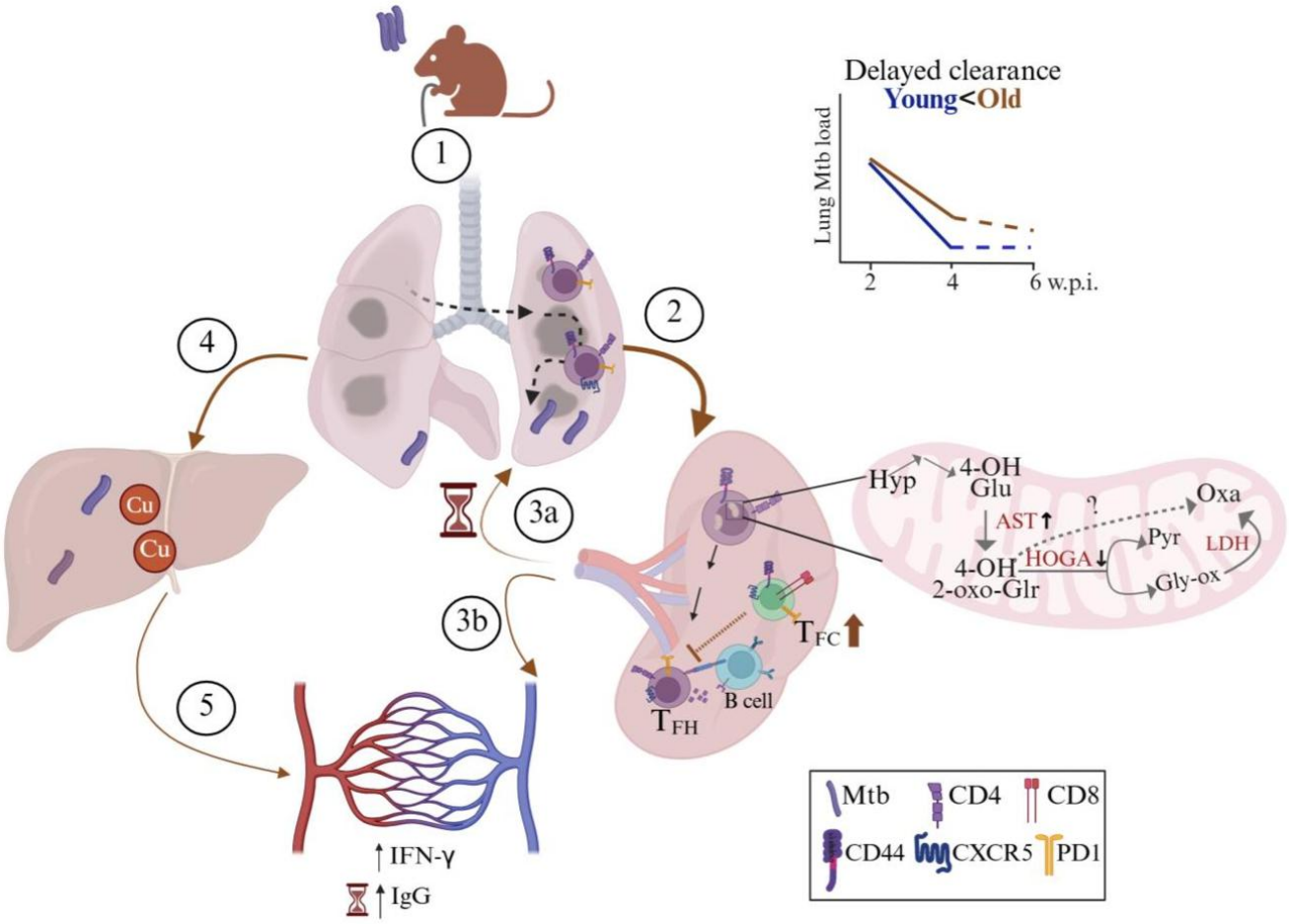

Figure 4. Age-associated mechanisms of delayed *Mycobacterium tuberculosis* lung clearance in old C57BL/6 mice during early rifampicin-isoniazid treatment. Illustrative summary of the results observed in the study. (1) Following Mtb infection via aerosol challenge, (2) antigen presentation takes place in the spleen. (3a) T cells reach the inflamed lung of old mice. (3b) Increased levels of proinflammatory cytokines: interferon-gamma (IFN-γ) and increased Mtb-specific IgG levels observed at later timepoint in Mtb-infected old mice. (4) Mtb disseminates to the liver via hepatic artery where copper (Cu) was observed to be accumulated (5) alongside increased systemic proinflammatory mediators. Old mice exhibit dysfunctional splenic T follicular helper (T_{FH} : $CD4^+CD44^+CXCR5^+PD1^+$) cells as a virtue of high T follicular cytotoxic cells (T_{FC} : $CD8^+CD44^+CXCR5^+PD1^+$), and leads to delayed lung Mtb clearance at 2 weeks post-treatment. Proteome analysis revealed splenic $CD4^+CD44^+$ T cells of old mice showed alterations in mitochondrial proteins (decreased HOGA: 4-hydroxy-2-oxoglutarate aldolase and increased AST), disrupting hydroxyproline (Hyp) degradation and promoting 4-hydroxy-2-oxo-glutarate (4-OH-2-oxo-Glr) accumulation, directing the reaction to oxalate (Oxa) via a pathway independent of lactate dehydrogenase (LDH), pyruvate (Pyr) and glyoxylate (Gly-ox). Created with BioRender.

This study has a few limitations. Technical constraints prevented direct proteomic profiling of lung T_{FH} cells, necessitating analysis of splenic $CD4^+CD44^+$ T cells as a functional proxy. Mouse models in TB research have limitations for extrapolating findings to humans due to differences in disease pathology, notably the absence of key features such as granuloma liquefaction, cavitation, and fibrosis. Also, mice exhibit different metabolic and aging patterns compared to humans, with distinct changes in organ metabolism, immune responses, and biomarkers of aging. Thus, age-associated metabolic alterations identified should be viewed as hypotheses for mechanisms that may operate in older humans, rather than as directly translatable biomarkers. Functional validation of mitochondrial defects including mitophagy flux assay, Seahorse bioenergetics or electron microscopy, remains a key next step. *In vitro* modulation of HOGA/AST (via inhibitors or overexpression) in T cells of lungs would test causality in rescuing anti-Mtb function. Future directions extend beyond T cell-intrinsic changes to dendritic cell antigen presentation and alterations in myeloid cell populations, and using clinical Mtb isolates in aging models for enhanced translational relevance.

In summary, this study demonstrated impaired pulmonary Mtb clearance in old C57BL/6 mice during RIF-INH treatment, driven by a confluence of immuno-senescence defects: inflammaging, delayed T_H1 responses, higher T_{FC} cell frequency and mitochondrial proteome collapse. These findings illuminate age-specific mechanisms contributing to suboptimal TB treatment responses in geriatric patients and identifying novel mitochondrial targets for adjunct therapy.

MATERIALS AND METHODS

Experimental groups, Mtb infection and treatment

The procedures adopted in this study were performed following the recommended Guidelines for Care and Use of Laboratory Animals and approved by the Animal Ethics Committee of ICGEB- New Delhi (Ref No. ICGEB/IAEC/07032020/TH-10). C57BL/6 mice of different age groups (2-, 4-, 9-, 12-, 17-, 19- and 31 months, M) were procured from the ICGEB bio-experimentation facility. The mice age equivalents to humans, used in this study, is as follows: young (2-4M), mid-aged (9-12M; 38-44 human years), old (17-19M; ~54-60 human years), and aged (31M; >80 human years) [7]. These mice were transferred to the BSL-III Tuberculosis Aerosol Challenge Facility (TACF) for experiments involving Mtb infection. Mice were fed a chow diet, water ad libitum and maintained at 20-22° C; 45-60% humidity with a 12h light/dark cycle. Mice were weight-adjusted, randomly grouped and after 1 week of acclimatization in TACF, infected with a low dose (100-120 cfu) of Mtb H37Rv strain in the Madison aerosol exposure chamber. After 2 w.p.i., a subset of mice received RIF and INH (100 mg/L each) in drinking water and fresh drug solutions were replaced every 48 hours. Two 17M mice (one bearing an abscess, the other died before the completion of 4 w.p.t.) were excluded from the study.

Cfu assay

Tissues (lung, spleen and liver) were homogenized in PBS (1 mL) and plated on 7H11 agar supplemented with Middlebrook 10% OADC. These plates were incubated at 37° C, and bacterial colonies were enumerated 3 weeks later.

Histopathology

Formalin-fixed lungs were paraffin-embedded, sectioned and stained with hematoxylin and eosin, followed by capturing images using Nikon Eclipse TS2. The slides were scored based on the severity of inflammation, granuloma formation and necrosis.

Liver micronutrient profiling

Liver (~50 mg) was subjected to microwave digestion post addition of H_2O_2 and HNO_3 (1:4). These were diluted and introduced to iCAP™-TQ ICP-MS using argon as carrier. Data acquisition was performed using Qtegra (Thermo Fisher Scientific, version 2.10.4345.39) and involved running different concentrations of a multielement standard mix (Supelco, #92091).

ALT and AST assay

Serum ALT and AST activities were measured using kits (Cayman Chemical, #700260 and #701640) according to the manufacturer's instructions.

Immune cell isolation and flow cytometry

Harvested tissues (lung and spleen) were incubated with collagenase D (1 µg/mL) and DNase I (0.5 mg/mL). Peripheral blood mononuclear cells (PBMCs) were isolated using Histopaque-1077 following standard procedures. Isolated cells were stained with recommended dilutions by the manufacturer: CD3-BV510 (BioLegend, #100234), CD4-BV785 (Bio-Legend, #100552), CD8a-AF700 (BioLegend, #100730), CD44-BV605 (BioLegend, #103047), CXCR5-PE/Dazzle 594 BioLegend, #145522), PD1-PE-Cy7 (BioLegend, #109110), KLRG1-BV421 (BioLegend, #138414), CD153-PE (BioLegend, #106405), CD25-AF488 (BioLegend, #102017) and CD127-BV650 (BioLegend, #135043) and LIVE/DEAD™ Fixable Near IR stain

(Invitrogen, #L34994) on ice for 45 min. After washing with buffer (0.2% FBS in 1× PBS), cells were treated with fixation (Invitrogen, #00-5123) and permeabilization buffer (Invitrogen, #00-8333) and kept on ice for 30 min. Intracellular staining was done with FoxP3-AF647 (BioLegend, #126408) and Tbet-BV711 (BioLegend, #644820) and incubated at RT for 45 min, followed by washing. Data (~1 million events/sample) was acquired using BD LSRFortessa X-20 and analyzed using FCS Express (DeNovo software, version 6).

Another set of immune cells were stained with: CD3-FITC (Invitrogen, #11-0032-82), CD4-SB600 (Invitrogen, #63-0042-82), CD8a-BV421 (BioLegend, #100753), CD44-BV510 (BioLegend, #103044), CXCR5-PE, ICOS-PerCP/Cy5.5 (BioLegend, #145504), PD1-PE-Cy7 (BioLegend, #109110) and LIVE/DEAD™ Fixable Near IR stain (Invitrogen, #L34994) on ice for 45 min. After washing with buffer (3% FBS in 1× PBS), splenic $CD4^+CD44^+$ T cells were sorted using BD FACS Aria III Fusion. Data was analyzed using FlowJo (BD Biosciences, version 10.8.1).

Lung IFN-γ estimation: IFN-γ was estimated in lung homogenates by using the ELISA MAX™ Standard Set Mouse IFN-γ kit (BioLegend, #430801) following the manufacturer's instructions.

Serum cytokine estimation

Two times diluted serum samples were used to estimate cytokines using capture bead-based assay LEGENDplex (BioLegend) along with the standard (BioLegend, #740371, lot no. B330381). The samples were acquired on BD LSRFortressa X-20 using PE and APC as the reporter and bead classification channel, respectively. Data was analyzed using Qognit software.

Serum IgG antibody quantification

ELISA plate was coated with Mtb H37Rv whole cell lysate (10 µg/mL) and incubated overnight at 4° C. Then, wash buffer (0.05% Tween-20 in 1× PBS) was added, followed by blocking in 3% BSA in 1× PBS containing 0.05% Tween-20 and incubated at 37° C for 2h at 180 rpm. After blotting the plate dry, sera were serially diluted fourfold in 0.1% BSA in 1× PBS containing 0.05% Tween-20, and 100 µL was added per well. The plate was then incubated overnight at 4° C. The plate was washed three times, followed by incubation with anti-mouse IgG (Southern Biotech, #1031-05) at 37° C for 2h at 180 rpm. The plate was washed six times and developed by adding o-phenylenediamine dihydrochloride, incubated at RT for 5 min. The reaction was terminated by adding 1N HCl, and the absorbance was measured at 490 nm.

Splenic $CD4^+CD44^+$ cell proteome analysis

Proteins were isolated using TRIzol reagent from sorted splenic $CD4^+CD44^+$ cells and quantified using BCA Protein Assay. An equal amount (~10 µg) of protein from each sample in a set (n = 10) was used for TMT10plex (Thermo Fisher Scientific, #90113). TMT-labelled peptides from all samples were pooled, dried and subjected to strong cation exchange chromatography and eluted using ammonium formate. Later, these fractions (n = 5) were cleaned up using C18 spin columns and dried, resuspended in formic acid (0.1%, 20 µL) and injected into an Orbitrap Fusion Lumos Tribrid Mass Spectrometer connected to a nano-LC 1200. Data was analysed with Proteome Discoverer version 2.3 using *Mus musculus* (ID: UP000000589; 55,087 protein count). Proteins qualifying the parameters [$\log_2$ fold change ≥ ± 0.58; $\log_{10}$p-value ≥1; false discovery rate<0.05] were selected as important deregulated molecules.

Statistical analysis

Data are presented as mean ± standard deviation. Details on the sample size and statistical analysis are provided in the figure legends.

Abbreviations

TB: tuberculosis; Mtb: *Mycobacterium tuberculosis*; RIF-INH: rifampicin and isoniazid; M: months; T_{FH}: T-follicular helper cells; T_{FC}: T-follicular cytotoxic cells; w.p.i.: weeks post infection; w.p.t.: weeks post treatment; ALT: alanine aminotransferase; AST: aspartate amino-transferase; HOGA: 4-hydroxy-2-oxoglutarate aldolase; PTGES3: Prostaglandin E synthase.

AUTHOR CONTRIBUTIONS

FP and RKN conceptualized the project. FP and SC carried out the mouse experiments and cytokine profiling. FP performed the flow cytometry data acquisition and prepared the liver micronutrient and proteomics samples. AG carried out antibody titers, ELISA experiments, and helped with proteomic data analysis. ShiC calculated histopathological scores. FP and RKN analyzed the data, wrote the original draft and revised it with the suggestions received from all the co-authors. RKN acquired funding, shared resources and administered the project. All co-authors reviewed and approved the manuscript.

ACKNOWLEDGEMENTS

Haripriya Priyadarsini, Adyasha Sarangi, Nidhi Yadav and Mothe Sravya are acknowledged for their help and

support during the mouse experiments. Help from Shilpa Sharma and Jaya Baranwal, and the staff of the bio-experimentation facility and the BSL-III Tuberculosis Aerosol Challenge Facility (TACF) at ICGEB-New Delhi, is acknowledged. DBT, Government of India supports the TACF. We thank Dr. Anmol Chandele for her insightful comments and suggestions for revising the manuscript. Part of these research findings were presented in Keystone Symposia on Molecular Basis of Healthy Aging in 2023; World Conference on Lung Health 2022, organized by The Union, and the 2nd biennial meeting on Sex Differences in the Immune Systems Conference in 2022, organized by Trinity College Dublin and Whitehead Institute. Some figures were created using BioRender.

CONFLICTS OF INTEREST

The authors declare that they have no conflicts of interest.

ETHICAL STATEMENT

The animal procedures adopted in this study were performed following the recommended Guidelines for Care and Use of Laboratory Animals and approved by the Animal Ethics Committee of ICGEB- New Delhi (Protocol No. ICGEB/IAEC/07032020/TH-10).

FUNDING

FP was supported with a Junior and Senior Research fellowship from the Department of Biotechnology (DBT), Government of India. SC was a Shyama Prasad Mukherjee Fellow supported by the Council of Scientific and Industrial Research, Government of India. A Senior Research Fellowship from the DBT supports AG. The core support from the International Centre for Genetic Engineering and Biotechnology (ICGEB), New Delhi, to RKN is highly acknowledged.

REFERENCES

1. Word Health Organization data website: https://www.who.int/news-room/fact-sheets/detail/ageing-and-health (Accessed 10/02/2024)

2. Yew WW, Yoshiyama T, Leung CC, Chan DP. Epidemiological, clinical and mechanistic perspectives of tuberculosis in older people. Respirology. 2018; 23:567–75. https://doi.org/10.1111/resp.13303 PMID:29607596

3. Bobak CA, Abhimanyu, Natarajan H, Gandhi T, Grimm SL, Nishiguchi T, Koster K, Longlax SC, Dlamini Q, Kahari J, Mtetwa G, Cirillo JD, O'Malley J, et al. Increased DNA methylation, cellular senescence and premature epigenetic aging in guinea pigs and humans with tuberculosis. Aging (Albany NY). 2022; 14:2174–93. https://doi.org/10.18632/aging.203936 PMID:35256539

4. Teo AK, Morishita F, Islam T, Viney K, Ong CW, Kato S, Kim H, Liu Y, Oh KH, Yoshiyama T, Ohkado A, Rahevar K, Kawatsu L, et al. Tuberculosis in older adults: challenges and best practices in the Western Pacific Region. Lancet Reg Health West Pac. 2023; 36:100770. https://doi.org/10.1016/j.lanwpc.2023.100770 PMID:37547037

5. Ku CC, Dodd PJ. Forecasting the impact of population ageing on tuberculosis incidence. PLoS One. 2019; 14:e0222937. https://doi.org/10.1371/journal.pone.0222937 PMID:31550293

6. Yen YF, Feng JY, Pan SW, Chuang PH, Su VY, Su WJ. Determinants of mortality in elderly patients with tuberculosis: a population-based follow-up study. Epidemiol Infect. 2017; 145:1374–81. https://doi.org/10.1017/S0950268817000152 PMID:28190404

7. Flurkey K, Currer JM, Harrison DE, Fox JG. The mouse in biomedical research. American College of Laboratory Animal Medicine series. Elsevier, AP: Amsterdam. 2007; 637–72. https://primo.qatar-weill.cornell.edu/permalink/974WCMCIQ_INST/lflmnj/alma991000123789706691

8. Cooper AM, Callahan JE, Griffin JP, Roberts AD, Orme IM. Old mice are able to control low-dose aerogenic infections with Mycobacterium tuberculosis. Infect Immun. 1995; 63:3259–65. https://doi.org/10.1128/iai.63.9.3259-3265.1995 PMID:7642254

9. Turner J, Frank AA, Orme IM. Old mice express a transient early resistance to pulmonary tuberculosis that is mediated by CD8 T cells. Infect Immun. 2002; 70:4628–37. https://doi.org/10.1128/IAI.70.8.4628-4637.2002 PMID:12117976

10. Vesosky B, Rottinghaus EK, Davis C, Turner J. CD8 T Cells in old mice contribute to the innate immune response to Mycobacterium tuberculosis via interleukin-12p70-dependent and antigen-independent production of gamma interferon. Infect Immun. 2009; 77:3355–63. https://doi.org/10.1128/IAI.00295-09 PMID:19470747

11. Jeyakumar SM. Micronutrient Deficiency in Pulmonary Tuberculosis - Perspective on Hepatic Drug Metabolism and Pharmacokinetic Variability of First-line Anti-Tuberculosis Drugs: Special Reference to Fat-soluble

Vitamins A, D, & E and Nutri-epigenetics. Drug Metab Lett. 2021; 14:166–76. https://doi.org/10.2174/1872312814999211130093625 PMID:34847853

12. Silva-Cayetano A, Fra-Bido S, Robert PA, Innocentin S, Burton AR, Watson EM, Lee JL, Webb LM, Foster WS, McKenzie RC, Bignon A, Vanderleyden I, Alterauge D, et al. Spatial dysregulation of T follicular helper cells impairs vaccine responses in aging. Nat Immunol. 2023; 24:1124–37. https://doi.org/10.1038/s41590-023-01519-9 PMID:37217705

13. Slight SR, Rangel-Moreno J, Gopal R, Lin Y, Fallert Junecko BA, Mehra S, Selman M, Becerril-Villanueva E, Baquera-Heredia J, Pavon L, Kaushal D, Reinhart TA, Randall TD et al. CXCR5^{+} T helper cells mediate protective immunity against tuberculosis. J Clin Invest. 2013; 123:712–26. https://doi.org/10.1172/JCI65728 PMID:23281399

14. Buchalski B, Wood KD, Challa A, Fargue S, Holmes RP, Lowther WT, Knight J. The effects of the inactivation of Hydroxyproline dehydrogenase on urinary oxalate and glycolate excretion in mouse models of primary hyperoxaluria. Biochim Biophys Acta Mol Basis Dis. 2020; 1866:165633. https://doi.org/10.1016/j.bbadis.2019.165633 PMID:31821850

15. Chen J, Deng JC, Zemans RL, Bahmed K, Kosmider B, Zhang M, Peters-Golden M, Goldstein DR. Age-induced prostaglandin E2 impairs mitochondrial fitness and increases mortality to influenza infection. Nat Commun. 2022; 13:6759. https://doi.org/10.1038/s41467-022-34593-y PMID:36351902

16. Dibbern J, Eggers L, Schneider BE. Sex differences in the C57BL/6 model of Mycobacterium tuberculosis infection. Sci Rep. 2017; 7:10957. https://doi.org/10.1038/s41598-017-11438-z Erratum in: Sci Rep. 2018; 8:6354. https://doi.org/10.1038/s41598-018-24598-3 PMID:28887521

17. Gupta M, Srikrishna G, Klein SL, Bishai WR. Genetic and hormonal mechanisms underlying sex-specific immune responses in tuberculosis. Trends Immunol. 2022; 43:640–56. https://doi.org/10.1016/j.it.2022.06.004 PMID:35842266

18. Hertz D, Dibbern J, Eggers L, von Borstel L, Schneider BE. Increased male susceptibility to Mycobacterium tuberculosis infection is associated with smaller B cell follicles in the lungs. Sci Rep. 2020; 10:5142. https://doi.org/10.1038/s41598-020-61503-3 PMID:32198367

19. Klein SL, Flanagan KL. Sex differences in immune responses. Nat Rev Immunol. 2016; 16:626–38. https://doi.org/10.1038/nri.2016.90 PMID:27546235

20. Márquez EJ, Chung CH, Marches R, Rossi RJ, Nehar-Belaid D, Eroglu A, Mellert DJ, Kuchel GA, Banchereau J, Ucar D. Sexual-dimorphism in human immune system aging. Nat Commun. 2020; 11:751. https://doi.org/10.1038/s41467-020-14396-9 PMID:32029736

21. Orme IM. Aging and immunity to tuberculosis: increased susceptibility of old mice reflects a decreased capacity to generate mediator T lymphocytes. J Immunol. 1987; 138:4414–8. PMID:3495592

22. Lafuse WP, Wu Q, Kumar N, Saljoughian N, Sunkum S, Ahumada OS, Turner J, Rajaram MVS. Psychological stress creates an immune suppressive environment in the lung that increases susceptibility of aged mice to Mycobacterium tuberculosis infection. Front Cell Infect Microbiol. 2022; 12:990402. https://doi.org/10.3389/fcimb.2022.990402 PMID:36189368

23. Toapanta FR, Ross TM. Impaired immune responses in the lungs of aged mice following influenza infection. Respir Res. 2009; 10:112. https://doi.org/10.1186/1465-9921-10-112 PMID:19922665

24. Lossow K, Kopp JF, Schwarz M, Finke H, Winkelbeiner N, Renko K, Meçi X, Ott C, Alker W, Hackler J, Grune T, Schomburg L, Haase H, et al. Aging affects sex- and organ-specific trace element profiles in mice. Aging (Albany NY). 2020; 12:13762–90. https://doi.org/10.18632/aging.103572 PMID:32620712

25. Rowland JL, Niederweis M. Resistance mechanisms of Mycobacterium tuberculosis against phagosomal copper overload. Tuberculosis (Edinb). 2012; 92:202-10. https://doi.org/10.1016/j.tube.2011.12.006 PMID:22361385

26. Sakiyama H, Fujiwara N, Yoneoka Y, Yoshihara D, Eguchi H, Suzuki K. Cu,Zn-SOD deficiency induces the accumulation of hepatic collagen. Free Radic Res. 2016; 50:666–77. https://doi.org/10.3109/10715762.2016.1164856 PMID:26981929

27. Cercamondi CI, Stoffel NU, Moretti D, Zoller T, Swinkels DW, Zeder C, Mhimibra F, Hella J, Fenner L, Zimmermann MB. Iron homeostasis during anemia of inflammation: a prospective study of patients with

tuberculosis. Blood. 2021; 138:1293–303. https://doi.org/10.1182/blood.2020010562 PMID:33876222

28. Orme IM, Griffin JP, Roberts AD, Ernst DN. Evidence for a defective accumulation of protective T cells in old mice infected with Mycobacterium tuberculosis. Cell Immunol. 1993; 147:222–9. https://doi.org/10.1006/cimm.1993.1062 PMID:7681730

29. Friedman A, Turner J, Szomolay B. A model on the influence of age on immunity to infection with Mycobacterium tuberculosis. Exp Gerontol. 2008; 43:275–85. https://doi.org/10.1016/j.exger.2007.12.004 PMID:18226868

30. Crotty S. T Follicular Helper Cell Biology: A Decade of Discovery and Diseases. Immunity. 2019; 50:1132–48. https://doi.org/10.1016/j.immuni.2019.04.011 PMID:31117010

31. Kim HJ, Verbinnen B, Tang X, Lu L, Cantor H. Inhibition of follicular T-helper cells by CD8(+) regulatory T cells is essential for self tolerance. Nature. 2010; 467:328–32. https://doi.org/10.1038/nature09370 PMID:20844537

32. Yu D, Ye L. A Portrait of CXCR5+ Follicular Cytotoxic CD8+ T cells. Trends Immunol. 2018; 39:965–79. https://doi.org/10.1016/j.it.2018.10.002 PMID:30377045

33. Sage PT, Tan CL, Freeman GJ, Haigis M, Sharpe AH. Defective TFH Cell Function and Increased TFR Cells Contribute to Defective Antibody Production in Aging. Cell Rep. 2015; 12:163–71. https://doi.org/10.1016/j.celrep.2015.06.015 PMID:26146074

34. Swanson RV, Gupta A, Foreman TW, Lu L, Choreno-Parra JA, Mbandi SK, Rosa BA, Akter S, Das S, Ahmed M, Garcia-Hernandez ML, Singh DK, Esaulova E, et al. Antigen-specific B cells direct T follicular-like helper cells into lymphoid follicles to mediate Mycobacterium tuberculosis control. Nat Immunol. 2023; 24:855–68. https://doi.org/10.1038/s41590-023-01476-3 PMID:37012543

35. Patel M, Yarlagadda V, Adedoyin O, Saini V, Assimos DG, Holmes RP, Mitchell T. Oxalate induces mitochondrial dysfunction and disrupts redox homeostasis in a human monocyte derived cell line. Redox Biol. 2018; 15:207–15. https://doi.org/10.1016/j.redox.2017.12.003 PMID:29272854

36. Headley CA, Gautam S, Olmo-Fontanez A, Garcia-Vilanova A, Dwivedi V, Akhter A, Schami A, Chiem K, Ault R, Zhang H, Cai H, Whigham A, Delgado J, et al. Extracellular Delivery of Functional Mitochondria Rescues the Dysfunction of CD4+ T Cells in Aging. Adv Sci (Weinh). 2024; 11:e2303664. https://doi.org/10.1002/advs.202303664 PMID:37990641

37. Headley CA, Gautam S, Olmo-Fontanez A, Garcia-Vilanova A, Dwivedi V, Schami A, Weintraub S, Tsao PS, Torrelles JB, Turner J. Mitochondrial Transplantation promotes protective effector and memory CD4+ T cell response during Mycobacterium tuberculosis infection and diminishes exhaustion and senescence in elderly CD4+ T cells. Adv Sci (Weinh). 2024; 11:e2401077. https://doi.org/10.1002/advs.202401077 PMID:39039808

SUPPLEMENTARY MATERIALS

Supplementary Figures

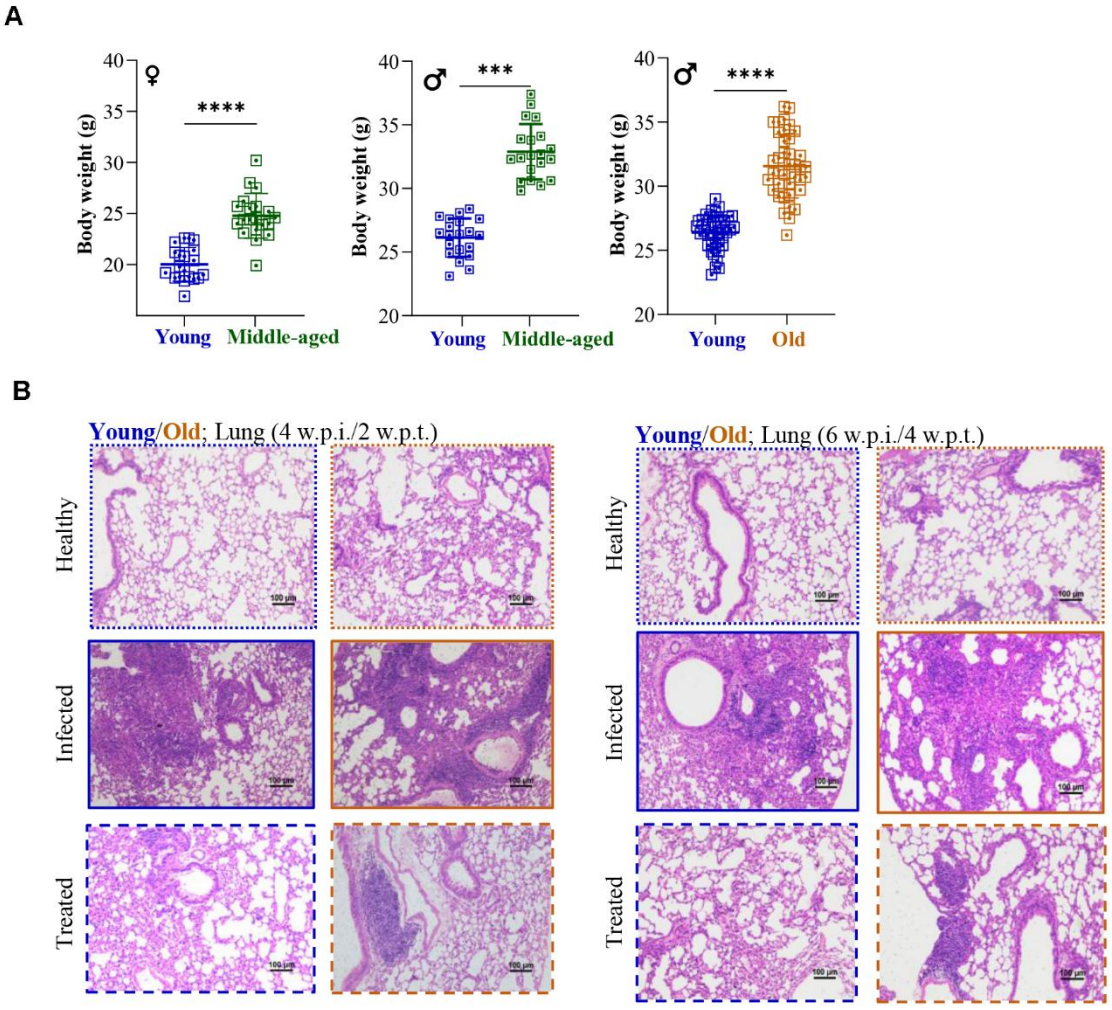

Supplementary Figure 1. Old C57BL/6 mice receiving two weeks of RIF-INH treatment showed delayed lung Mtb clearance. (**A**) Body weight (in gram) of mice (n=20/age group for young and middle-aged panels, n=40/age group for young and old panel) prior to infection (day -5). (**B**) Lung histopathological images (hematoxylin and eosin; H&E stained, 100× magnification, scale bar=100 μm) at 4 w.p.i./2 w.p.t. and 6 w.p.i./4 w.p.t. Young (2-4 months) in blue, middle-aged (9-12 months) in green and old (17-19 months) mice in brown; w.p.i.: weeks post infection; w.p.t.: weeks post treatment; p-values: *** <0.0005 and **** <0.0001 at 95% confidence interval by Mann-Whitney test. Data shown as mean ± SD. *See also Figures 1, 2.*

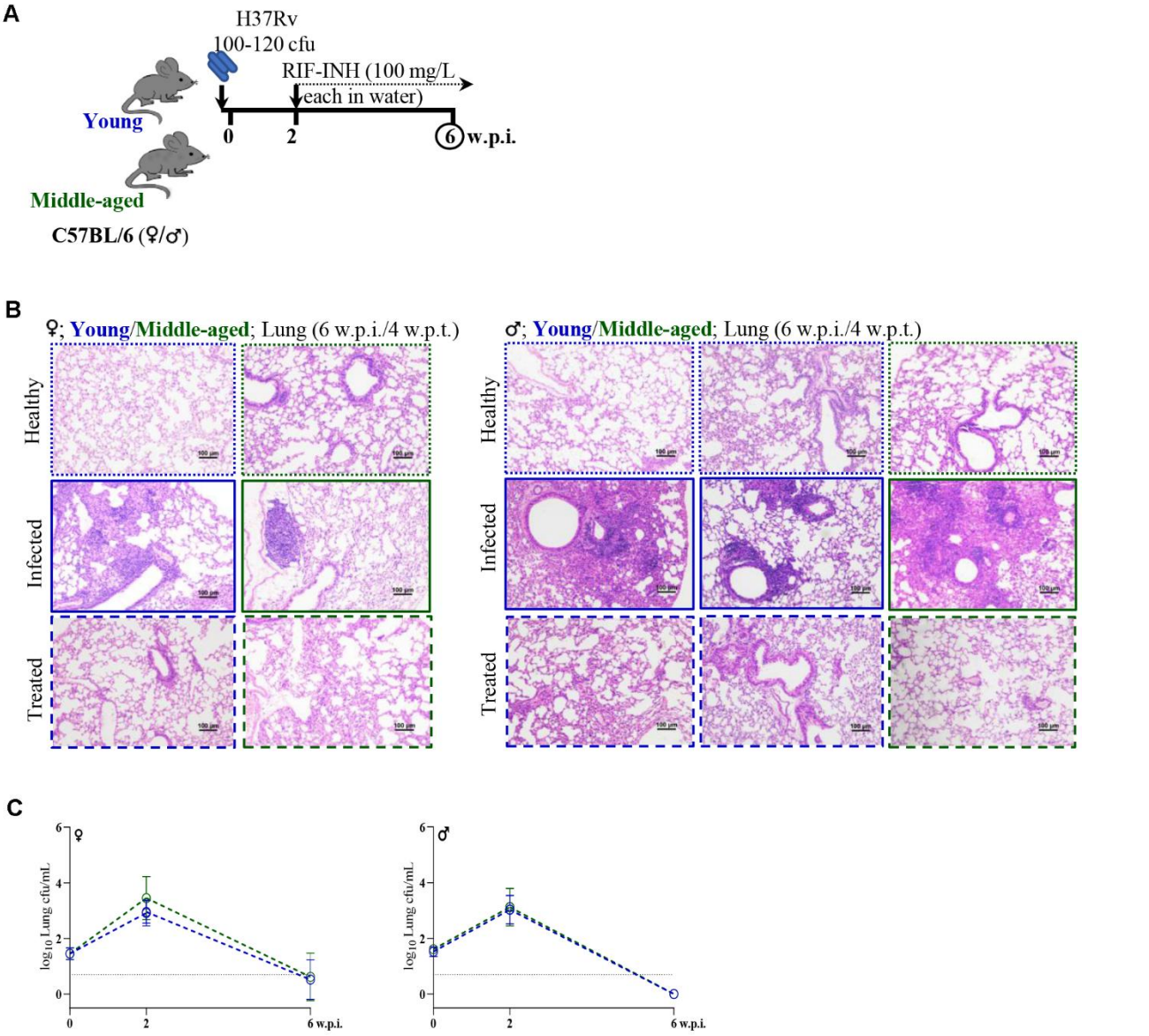

Supplementary Figure 2. Middle-aged C57BL/6 mice showed similar treatment outcomes post Mtb infection compared to younger mice irrespective of gender. (**A**) Schematic of the experimental design for Mtb H37Rv infection and RIF-INH treatment of C57BL/6 mice (female: age groups of 2 and 9 months and male: age groups of 2 and 12 months; M). (**B**) Lung histopathological images (hematoxylin and eosin: H&E stained, 100× magnification, scale bar=100 μm) at 6 w.p.i./4 w.p.t. along with their respective healthy controls. *One set of images of the young mice group at 6 w.p.i./4 w.p.t. was also shown in Supplementary Figure 1B, as a part of the same infection experiment.* (**C**) Lung bacterial burden (in log10cfu/mL) in mice belonging to treated group (at 4 w.p.t.; treatment started at 2 w.p.i.) groups; n=5/timepoint/age group/condition; dashed horizontal line represents limit of detection. Young (2 months) mice in blue and middle-aged (9-12 months) mice in green; cfu: colony forming unit; w.p.i.: weeks post infection; w.p.t.: weeks post treatment. Data shown as mean ± SD. *See also Figure 1.*

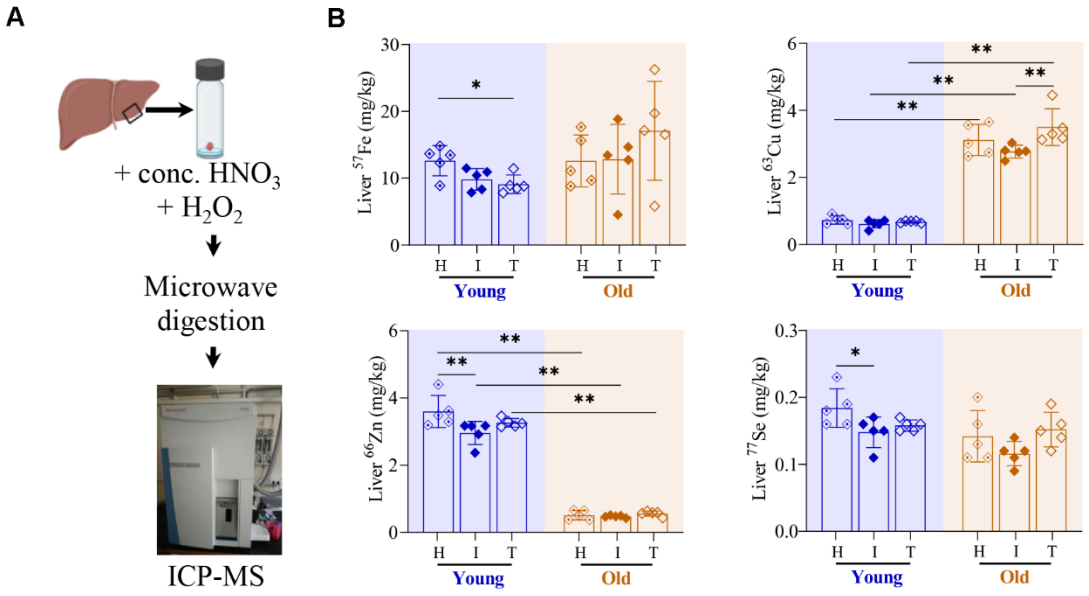

Supplementary Figure 3. Impaired Mtb clearance in old C57BL/6 mice potentially correlates with abnormal levels of liver micronutrients. (**A**) Method adopted for liver micronutrient profiling by inductive coupled plasma mass spectrometry (ICP-MS). (**B**) Abundance of mice liver micronutrients (in milligram per kilogram): iron- ^{57}Fe, copper- ^{63}Cu, zinc- ^{66}Zn, and selenium- ^{77}Se of healthy (H), Mtb H37Rv infected (I) and RIF-INH treated (T) groups at 4 w.p.i./2 w.p.t.; n=5/age group/condition. p-values: * ≤0.05 and ** <0.005 at 95% confidence interval by Mann- Whitney test. Data shown as mean ± SD. Young (2 months) in blue and old (17 months) mice in brown.

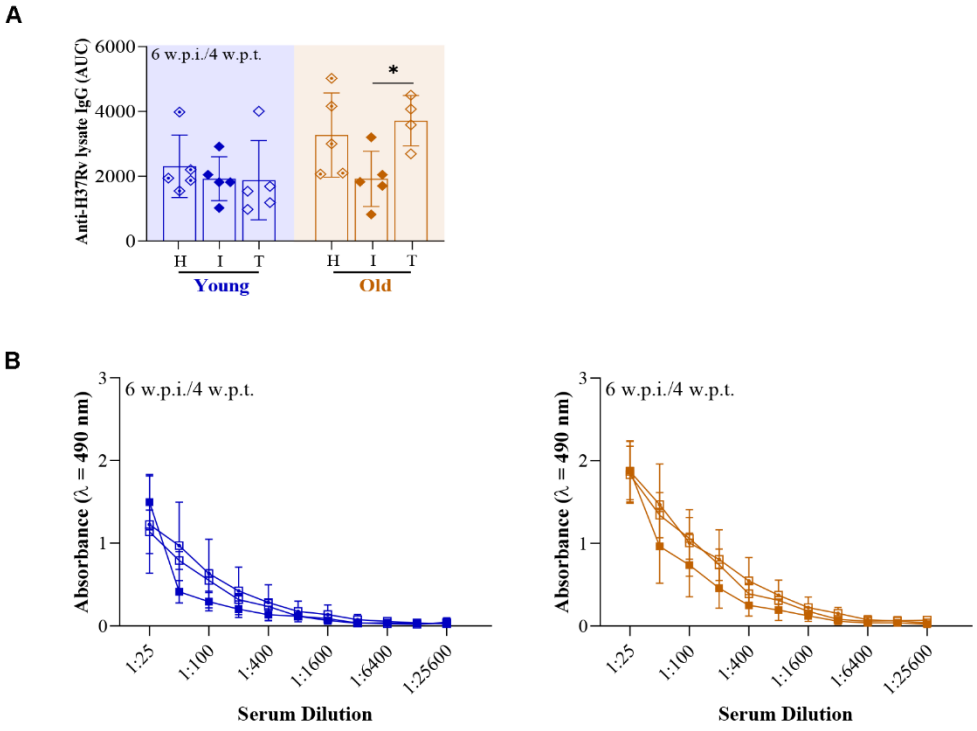

Supplementary Figure 4. Serum anti-Mtb IgG was higher in old mice after RIF-INH treatment. (**A**) Anti-H37Rv lysate IgG estimation with area under the curve (AUC) in the circulation of healthy (H), Mtb H37Rv infected (I) and RIF-INH treated (T) C57BL/6 mice at 6 w.p.i./4 w.p.t.. (**B**) End-point serum dilutions to monitor anti-IgG titers in mice groups at 6 w.p.i./4 w.p.t.; n = 5/time point/age group/condition (only old-T had n=4 at 4 w.p.t.). Young (2 months) in blue and old (17 months) mice in brown; p-value: * ≤0.05 at 95% confidence interval by Mann-Whitney test. Data shown as mean ± SD. *See also Figure 2.*

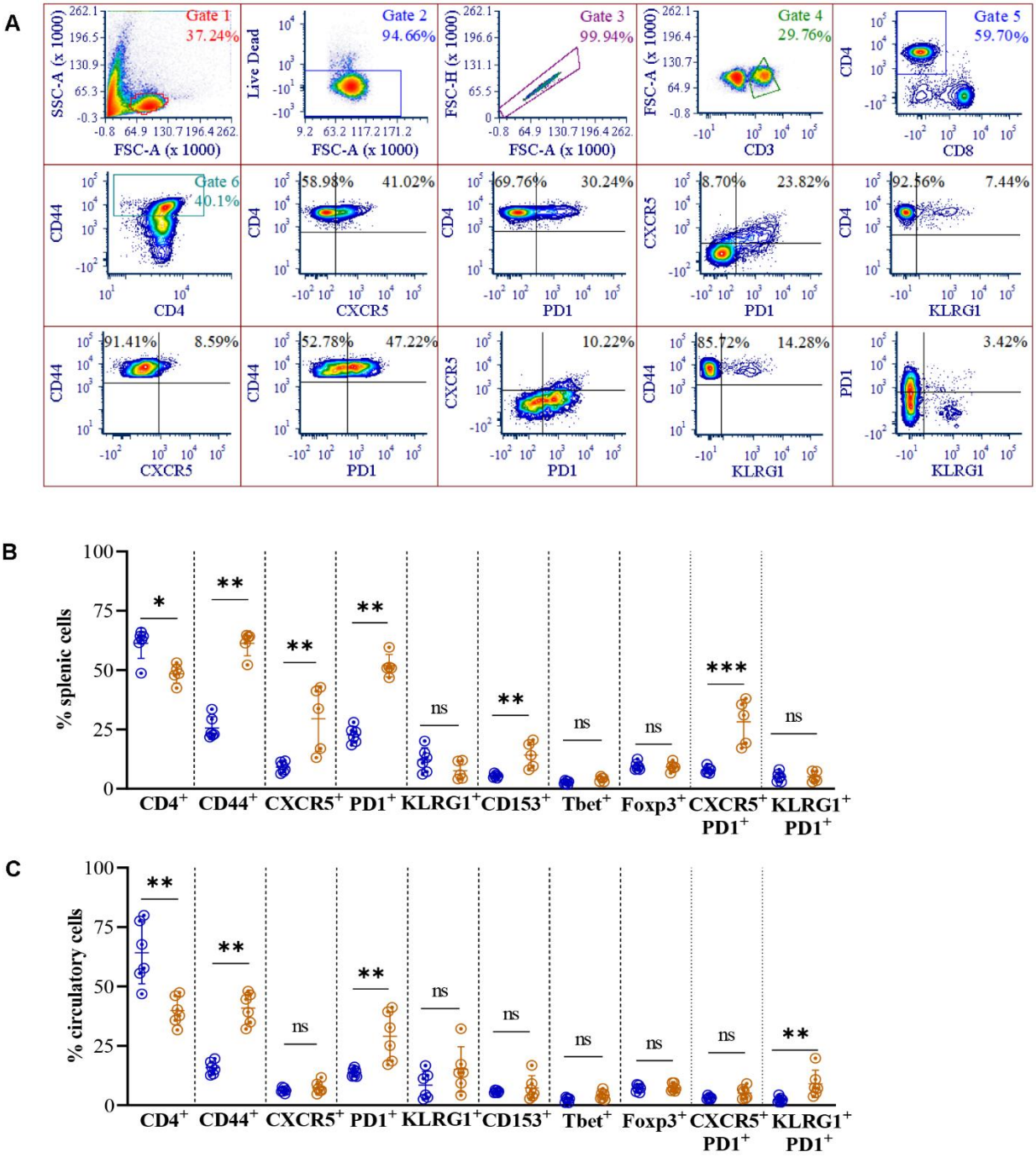

Supplementary Figure 5. Splenic and circulatory CD4+ T cell subsets frequency altered in old C57BL/6 mice. (**A**) Gating strategy in the lung of a representative mouse adopted to monitor the frequency of multiple CD4+ T cell subsets; *data analyzed using FCS Express (version 6).* Frequency of CD4+, CD4+CD44+, CD4+CXCR5+, CD4+PD1+, CD4+KLRG1+, CD4+CD153+, CD4+Tbet+, CD4+CD25+CD127-FoxP3+, CD4+CXCR5+PD1+ and CD4+KLRG1+PD1+ cells in the (**B**) spleen and (**C**) circulation of healthy mice are presented. n = 6 for young, n = 5-6 for old mice; Young (2 months) in blue and old (17 months) mice in brown; p-values: ns= non-significant, * ≤0.05, ** <0.005 and *** <0.0005 at 95% confidence interval by Mann-Whitney test. Data shown as mean ± SD.

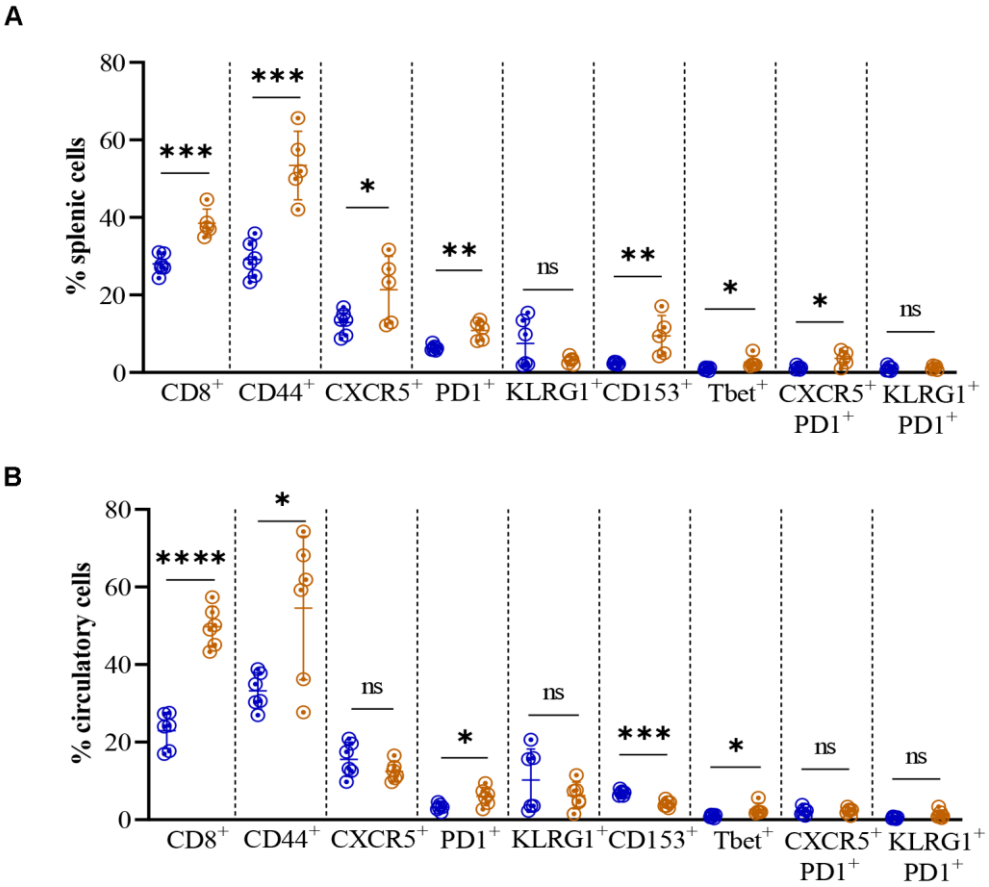

Supplementary Figure 6. Splenic and circulatory CD8+ cells subsets altered in old mice. Frequency of CD8+, CD8+CD44+, CD8+CXCR5+, CD8+PD1+, CD8+KLRG1+, CD8+CD153+, CD8+Tbet+, CD8+CXCR5+PD1+, CD8+KLRG1+PD1+cells in the (**A**) spleen and (**B**) circulation of healthy young (n=6) and old (n=5-6) mice are presented. Young (2 months) in blue and old (17 months) mice in brown; p-values: ns = non-significant, * ≤0.05, ** <0.005, *** <0.0005 and **** <0.0001 at 95% confidence interval by Mann- Whitney test. Data is represented as mean ± SD.

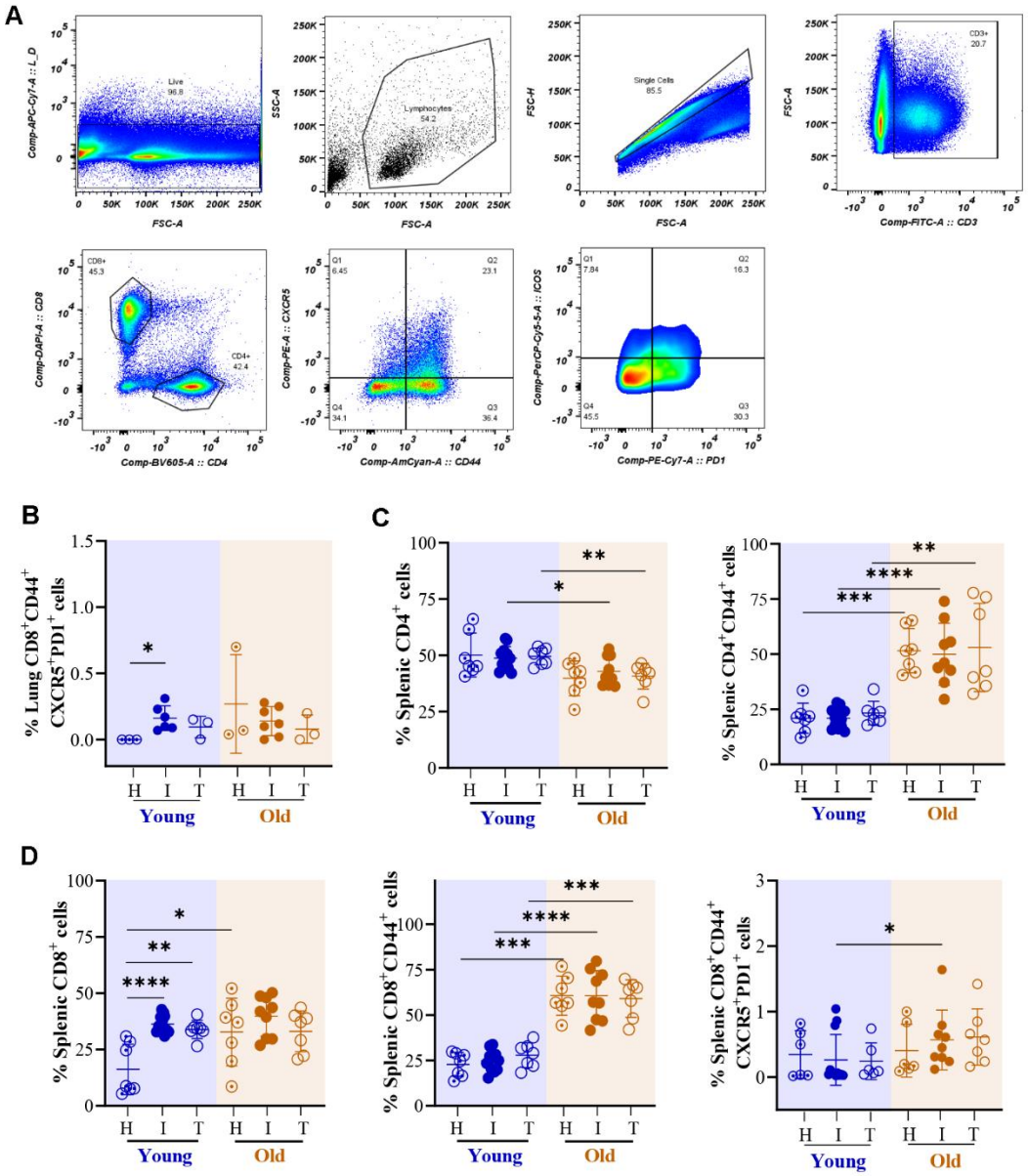

Supplementary Figure 7. Higher lung and splenic CD8+CD44+CXCR5+PD1+ cells observed in Mtb infected old mice. (**A**) Gating strategy of a representative mouse adopted to monitor the frequency of T cell subsets in the lung of C57BL/6 mice; *data analyzed using FlowJo (version 10.8).* (**B**) Frequency of lung CD8+CD44+CXCR5+PD1+ cells of healthy (H, n=3/age group), Mtb H37Rv infected (I, n= 9-10/age group) and RIF-INH treated (T, n=3/age group) C57BL/6 mice at 4 w.p.i./2 w.p.t.. Frequency of splenic (**C**) CD4+ and CD4+CD44+ (**D**) CD8+, CD8+CD44+ and CD8+CD44+CXCR5+PD1+ cells of healthy (H, n=6-7/age group), Mtb H37Rv infected (I, n=9-12/age group) and RIF-INH treated (T, n=6-7/age group) C57BL/6 mice at 4 w.p.i./2 w.p.t. Young (2-4 months) in blue and old (17-19 months) mice in brown; p-values: * ≤0.05, ** <0.005, *** <0.0005 and **** <0.0001 at 95% confidence interval by Mann-Whitney test. Data shown as mean ± SD. *See also Figure 3.*

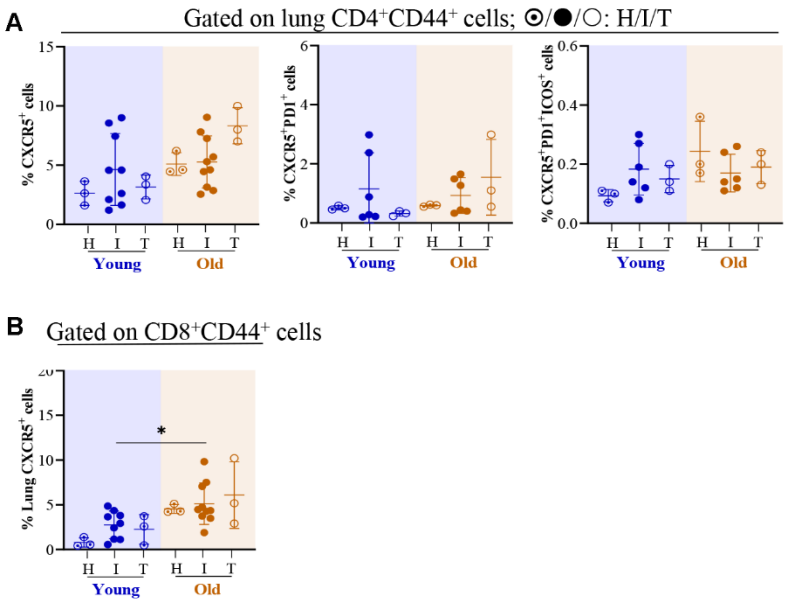

Supplementary Figure 8. Lung CD8+CD44+CXCR5+ cells were higher in old C57BL/6 mice post Mtb infection. (**A**) Frequency of CD4+CD44+CXCR5+, CD4+CD44+CXCR5+PD1+ and CD4+CD44+CXCR5+PD1+ICOS+ cells in the lungs of C57BL/6 mice at 4 w.p.i./2 w.p.t. are presented. (**B**) Frequency of CD8+CD44+CXCR5+ cells in the lungs and spleen at 4 w.p.i./2 w.p.t. are presented. Healthy (H, n=3/age group), Mtb H37Rv infected (I, n= 6-10/age group) and RIF-INH treated (T, n=3/age group). Young (2- 4 months) in blue and old (17-19 months) mice in brown; p-value: * ≤0.05 at 95% confidence interval by Mann-Whitney test. Data shown as mean ± SD. *See also Figure 3.*

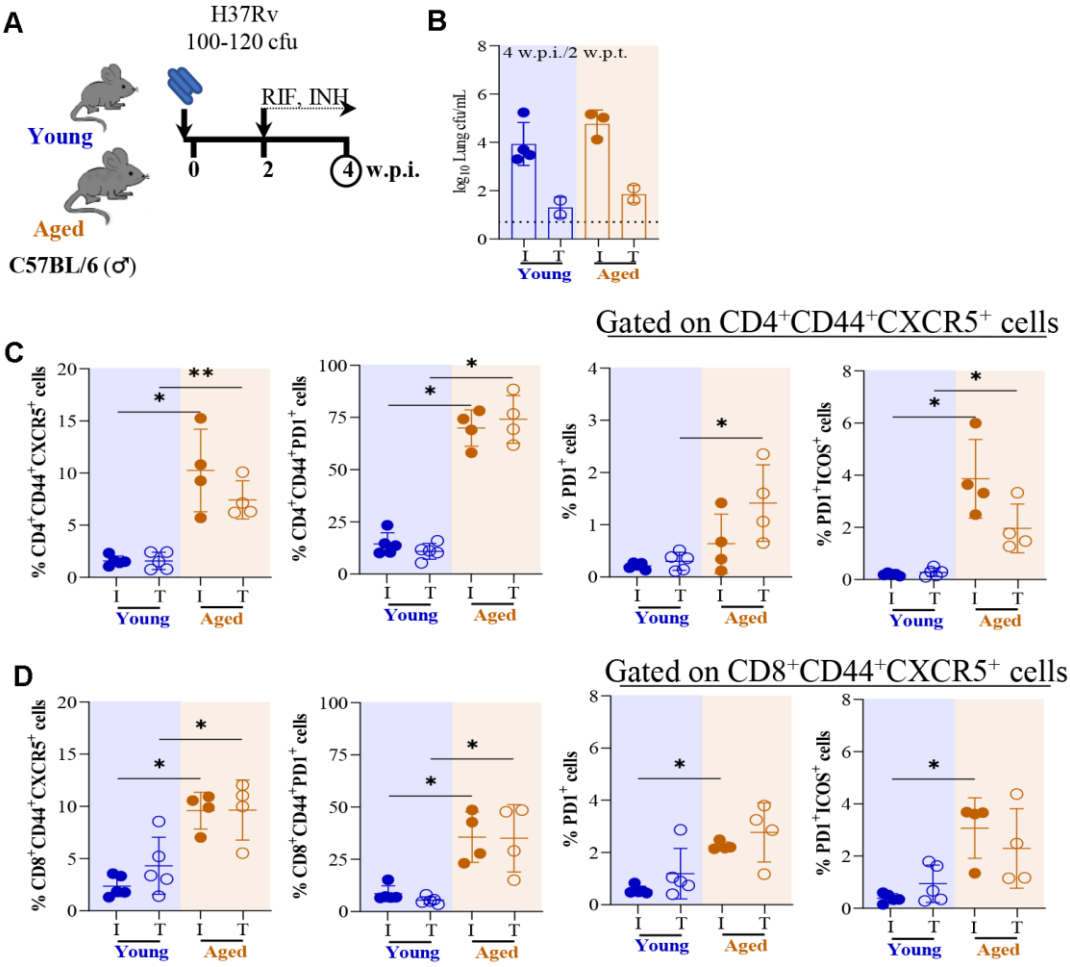

Supplementary Figure 9. Higher splenic CD4+CD44+CXCR5+ cells observed in aged mice. (**A**) Schematic of the experimental design for Mtb H37Rv infection and RIF-INH treatment of male C57BL/6 mice. (**B**) Lung bacterial burden (in log10cfu/mL) of Mtb infected mice (at 4 w.p.i.) and RIF-INH treated mice (at 2 w.p.t.; treatment started at 2 w.p.i.); dashed horizontal line represents limit of detection (LOD); Infected (I) mice: n=3-4 for young and old; Treated (T) mice: n=2 for young and old; rest cfu data points could not be collected due to plate contamination. (**C**) Frequency of splenic CD4+CD44+CXCR5+, CD4+CD44+PD1+, CD4+CD44+CXCR5+PD1+ and CD4+CD44+CXCR5+PD1+ICOS+ cells of I and T groups of mice at 4 w.p.i./2 w.p.t. (**D**) Frequency of splenic CD8+CD44+CXCR5+, CD8+CD44+PD1+, CD8+CD44+CXCR5+PD1+ and CD8+CD44+CXCR5+PD1+ICOS+ cells of I and T groups of mice at 4 w.p.i./2 w.p.t. n=4-5/condition; Young (2 months) in blue and aged (31 months) mice in brown; p-values: * ≤0.05 and ** <0.005 at 95% confidence interval by Mann-Whitney test. Data shown as mean ± SD.

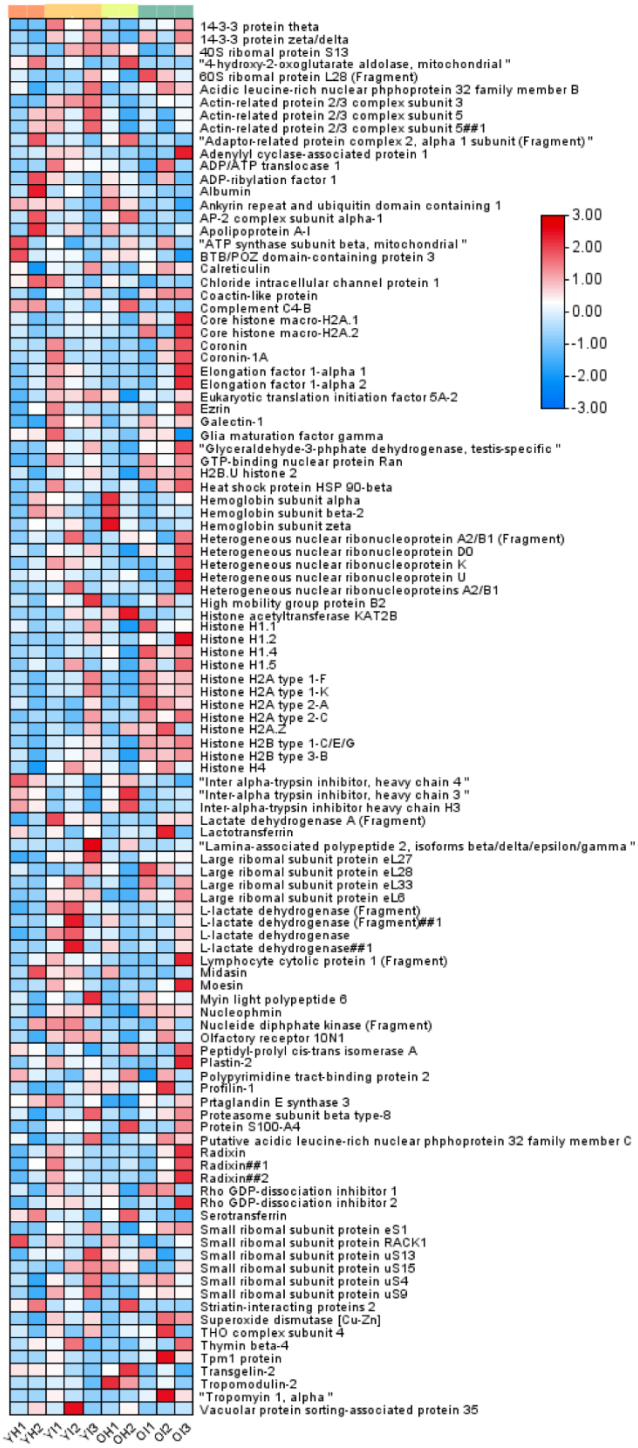

Supplementary Figure 10. Proteome distribution of CD4+CD44+ T cells changed upon Mtb infection. Heatmap showing abundance of identified splenic CD4+CD44+ T cell proteins obtained from TMT10plex experiment using healthy (H) and Mtb H37Rv infected (I) C57BL/6 mice groups (Y: young, 4 months) and (O: old, 19 months). Each row presents abundance of individual protein. 1,2,3 shows the biological replicates. Colour intensity indicates the abundance values. *See also Figure 3.*

Supplementary Tables

Please browse Full Text version to see the data of Supplementary Tables 3, 4.

Supplementary Table 1. Compiled results of the study. Distribution of different immune cells in young (2M, 4M), old (17M, 19M) and aged (31M) male C57BL/6 mice in (A) spleen of healthy (H), Mtb H37Rv infected (I) and RIF-INH treated (T) groups at 4 w.p.i./2 w.p.t. and in (B) lung of Mtb infected mice at 4 w.p.i.; M: months. ***See also Figure 3.***

A

Splenic cells	Condition	2M	4M	17M	19M	31M
$CD4^+$	H	58±9	43±2	45±4	37±8	N/A
	I	55±2	46±3	47±6	40±5	42±5
	T	49±5	49±4	43±4	41±7	43±9
$CD4^+CD44^+$	H	25±4	17±4	61±5	49±10	N/A
	I	23±2	20±5	65±9	42±8	88±5
	T	21±2	23±6	73±5	37±4	86±6
$CD4^+CD44^+CXCR5^+$	H	3±0.5	4±2.6	6±1.4	14±10	N/A
	I	4±0.3	4±2.3	8±1.5	16±3	10±4
	T	2±1.6	10±3	6±3.2	23±4	7.4±1.8
$CD4^+CD44^+CXCR5^+PD1^+$	H	3.8±1.3	1±0.7	8±4.7	3.4±2	N/A
	I	4.5±1.4	1±0.6	16±11	4.7±0.8	0.6±0.5
	T	3.8±1.2	1.3±0.1	9±3.3	5.8±1.2	1.4±0.7
$CD8^+$	H	28±2	14±13	38±4	29±16	N/A
	I	34±3	37±4	32±7	44±7	46±5
	T	29±4	35±3	24±4	40±2	42±7
$CD8^+CD44^+$	H	28±1	18±4	60±5	60±13	N/A
	I	29±3	23±5	56±20	62±11	77±9
	T	20±2	31±5	53±14	63±3	71±16
$CD8^+CD44^+$ $CXCR5^+$	H	1.6±1	1.6±0.9	0.5±0.1	6±3	N/A
	I	1±0.4	2.4±1.5	4±2	8.4±3.5	9.6±1.7
	T	1.5±0.8	5±2	2±3	7.6±2.3	9.6±2.8
$CD8^+CD44^+CXCR5^+PD1^+$	H	0.6±0.2	0.02±0.01	1.7±1	0.2±0.3	N/A
	I	0.9±0.1	0.05±0.02	1.7±1.6	0.3±0.1	2.3±0.1
	T	0.5±0.2	0.07±0.03	0.9±0.4	0.3±0.2	2.8±1.2

B

Lung cells	2M	4M	17M	19M
$CD4^+$	28±6	41±8	26±2	48±13
$CD4^+CD44^+$	47±1	65±5	75±4	69±9
$CD4^+CD44^+CXCR5^+$	3±1	4±3	3.6±1.7	5±2
$CD4_+CD44^+CXCR5^+PD1^+$	6±3	1.1±1	2±1	0.8±0.6
$CD8^+$	17±3	32±9	18±4	30±7
$CD8^+CD44^+$	45±15	57±10	82±4	64±15
$CD8^+CD44^+CXCR5^+$	0.9±0.3	3.6±0.9	6±3	4.3±1.7
$CD8^+CD44^+CXCR5^+PD1^+$	4±2	0.16±0.1	2±1	0.14±0.1

Supplementary Table 2. Total number of sorted activated splenic CD4+ T cells and their protein amount from healthy young (4 months) and old (19 months) C57BL/6 mice upon Mtb H37Rv infection and RIF -INH treatment. ***See also Figure 3.***

Mice Condition	Number of $CD4^+$ $CD44^+$ cells sorted	Total protein amount (µg)
Healthy (Young)	4,31,308	24.53
	3,23,580	13.96
	4,41,483	9.06
	4,35,189	20.38
Mtb-infected (Young)	5,82,869	15.47
	3,50,937	6.79
	3,00,415	6.42
	2,80,196	16.60
	1,63,427	7.17
	2,00,368	20.00
RIF-INH treated (Young)	2,47,515	13.58
	3,20,773	24.91
	6,49,437	18.11
	1,36,499	1.13
	5,18,395	6.79
	5,34,188	10.94
	3,61,425	15.47
Healthy (Old)		
	10,17,677	19.25
	6,63,651	13.21
Mtb-infected (Old)	4,55,972	8.30
	4,37,661	14.72
	4,28,506	12.45
	6,22,087	20.38
	6,84,220	10.94
	3,67,149	10.57
RIF-INH treated (Old)	7,38,297	6.79
	3,66,620	36.23
	1,99,573	36.60
	3,51,695	8.68

Supplementary Table 3. List of identified proteins (n= 109) from splenic $CD4^+CD44^+$ T cells (TMT- Set 1) showing Mtb H37Rv infected young and old C57BL/6 mice with their respective healthy controls. Y: young (4 months); O: old (19 months); I: Mtb infected; H: Healthy. See also Figure 3.

Supplementary Table 4. List of identified proteins (n=41) from splenic $CD4^+CD44^+$ T cells (TMT- Set 2) showing RIF-INH treated young and old C57BL/6 mice with Mtb H37Rv infected controls. Y: young (4 months); O: old (19 months); T: RIF-INH treated; I: Mtb infected. See also Figure 3.